arXiv:1511.04953v2 [astro-ph.SR] 20 Nov 2015

Accepted for publication in The Astrophysical Journal

The evolved pulsating CEMP star HD 112869

Laimons Začs[1,2], Julius Sperauskas[1], Aija Grankina[2], Viktoras Deveikis[1], Bogdan Kaminskyi[3], Yakiv Pavlenko[3], and Faig A.Musaev[4,5,6]

ABSTRACT

Radial velocity measurements, BVR_C photometry, and high-resolution spectroscopy in the wavelength region from blue to near infrared are employed in order to clarify the evolutionary status of the carbon-enhanced metal-poor star HD 112869 with unique ratio of carbon isotopes in the atmosphere. An LTE abundance analysis was carried out using the method of spectral synthesis and new self consistent 1D atmospheric models. The radial velocity monitoring confirmed semiregular variations with a peak-to-peak amplitude of about 10 km s^{-1} and a dominating period of about 115 days. The light, color and radial velocity variations are typical of the evolved pulsating stars. The atmosphere of HD 112869 appears to be less metal-poor than reported before, [Fe/H] = -2.3 ± 0.2 dex. Carbon to oxygen and carbon isotope ratios are found to be extremely high, C/O $\simeq$ 12.6 and $^{12}C/^{13}C \gtrsim 1500$, respectively. The s–process elements yttrium and barium are not enhanced, but neodymium appears to be overabundant. The magnesium abundance seems to be lower than the average found for CEMP stars, [Mg/Fe] $< +0.4$ dex. HD 112869 could be a single low mass halo star in the stage of asymptotic giant branch evolution.

Subject headings: stars: carbon – stars: AGB and post-AGB – stars: abundances – stars: oscillations – stars: individual: TT CVn

[1]Vilnius University Observatory, Čiurlionio 29, Vilnius 2009, Lithuania

[2]Laser Center, University of Latvia, Raiņa bulvāris 19, LV-1586 Rīga,Latvia

[3]Main Astronomical Observatory of Academy of Sciences of Ukraine, Zabolotnoho 27, Kyiv, 03680, Ukraine

[4]Special Astrophysical Observatory of the Russian AS, Nizhnij Arkhyz, 369167, Russia

[5] Institute of Astronomy of the Russian AS, 48 Pyatnitskaya st., 119017, Moscow, Russia

[6] Terskol Branch of Institute of Astronomy of the Russian AS, 361605 Peak Terskol, Kabardino-Balkaria, Russia

1. Introduction

The wide-field spectroscopic surveys revealed high frequency of carbon-enhanced stars with [C/Fe] > 1.0 (hereafter CEMP stars) among metal-poor stars (Beers et al. 1992; Christlieb et al. 2001). According to Lucatello et al. (2005); Lucatello (2006), up to 30 percents of stars with [Fe/H] < –2.5 are carbon-rich. The chemical abundances of CEMP stars reflect the origin of CNO and neutron capture elements in the early Galaxy. CEMP stars have a wide variety of elemental abundance patterns **(see Beers et al. (2007); and references therein)**. The majority of CEMP stars have enhanced s-process elements (Aoki et al. 2007) and are referred to as CEMP-s stars. Other CEMP stars exhibit strong enhancements of r-process elements (CEMP-r) or the presence of enhanced neutron-capture elements associated with both the r- and s−processes (CEMP-r/s). The class of CEMP-no stars comprises stars that, in spite of high carbon (and often N and O) overabundances with respect to Fe, do not exhibit strong neutron-capture elements. Recently, CEMP stars have also been found with large enhancements of α-elements (Norris et al. 2001; Aoki et al. 2002; Depagne et al. 2002), which Aoki et al. (2006) refer to as CEMP-α stars.

Observed CEMP stars bear signatures of thermally pulsating asymptotic giant branch (TP-AGB) and explosive nucleosynthesis in the early Galaxy and subsequent mixing or mass transfer in single or binary stars (see Masseron et al. (2010); and references therein). The carbon in the CEMP-s stars is very likely to have been produced by an intermediate-mass asymptotic giant branch (AGB) companion that has transferred material to the currently observed star. Bisterzo et al. (2011) suggest that all CEMP-s stars observed until now are old halo main sequence and turn-off stars or giants of a low initial mass (M $< 0.9 M_{\odot}$). The origin of the carbon in the other CEMP classes is not yet fully understood. The CEMP-no stars are of special interest because the observed CNO elements probably have been produced by a primordial population of massive ($20 < M/M_{\odot} < 100$) and megametal-poor ([Fe/H] < –6) stars, which are predicted to have experienced significant mass loss of CNO-enhanced material via strong winds (Hirschi 2007; Meynet et al. 2006). Alternatively, the carbon excess at extremely low metallicity may have been produced by the ejecta of the so-called faint supernovae (Umeda & Nomoto 2005).

A high $^{12}C/^{13}C$ ratio is observed rarely among the analyzed CEMP stars. The CEMP-no stars exhibit quite low $^{12}C/^{13}C$ ratios (in the range $4 < {}^{12}C/{}^{13}C < 10$), indicating that a significant amount of mixing has occurred in their progenitor objects (Aoki et al. 2007; Sivarani et al. 2006). Strong mixing occurs on the red giant branch due to the first dredge-up (FDU) affecting carbon and nitrogen abundances and decreasing the $^{12}C/^{13}C$ ratio. However, it is not sufficient to explain the low isotopic ratios $^{12}C/^{13}C < 30$ observed for most of the studied CEMP-s and CEMP-r/s stars (see Bisterzo et al. (2011); and references therein).

Further extra-mixing has to be hypothesized during the following AGB phase to interpret the observations. Cool bottom processing (CBP) may explain the observed [C/Fe] and [N/Fe]. According to Bisterzo et al. (2011), most of the studied CEMP-s and CEMP-r/s stars need the occurrence of CBP to describe the observed abundance patterns. The observed [C/Fe] ratios agree with AGB predictions without involving of extra-mixing only in four stars: CS22880−074, CS30315−91, HE0507−1653, and HE1429−0551. The first two stars show, in addition, relatively high lower limits for $^{12}C/^{13}C$ (>40–60). HD 13826 (= V Ari) is an exception, with high $^{12}C/^{13}C$ ratio found by Kipper & Kipper (1990) and confirmed by Aoki & Tsuji (1997) and Beers et al. (2007), $^{12}C/^{13}C = 90 \pm 10$. Tsuji et al. (1991) and Kipper (1992) detected another metal poor star, HD 112869 (= TT CVn), with an extremely low intensity of molecular lines with isotopic ^{13}C.

HD 112869 is a high latitude (b = +79°) extremely metal-poor ([Fe/H] = −2.9; Kipper Kipper (1992)) star classified as R type carbon star with enhanced CH bands by Keenan & Morgan (1941). The bolometric magnitude estimated by Bergeat et al. (2002), M_{bol} = –3.35 mag, is in a good agreement with an independent estimation provided by Eggen (1972), M_{bol} = –3.5 mag. Estimation of the trigonometric distance is not possible because of a negative parallax value for HD 112869, $\pi = -1.26 \pm 1.28$ mas (van Leeuwen 2007). Effective temperature for HD 112869 was determined by means of the infrared flux method (IRFM), which uses the ratio of bolometric flux to the infrared flux in L band, $T_{\rm eff}$ = 3715 K (Aoki & Tsuji 1997). The effective temperature found by Bergeat et al. (2001) using the same method is a bit higher, T_{eff} = 3870 K. Tanaka et al. (2007) calculated the effective temperature, T_{eff} = 4100 K, by fitting the near infrared spectra at wavelengths of 1.35, 1.74, and 2.29 μm, where the molecular absorption because of CO, CN, and C_2 is relatively low, with the model spectra. Surface gravity, $\log g = 0.4$ (cgs), was estimated by Kipper (1992) using the well known relation between $\log g$, T_{eff}, stellar mass (M), and M_{bol}, assuming for the star $1M_{\odot}$. Aoki & Tsuji (1997) used for spectral synthesis two different values of $\log g$, 0.0 and 2.0 (cgs). The microturbulent velocity (ξ_t) was estimated iteratively using the profiles of molecular lines (Kipper 1992) and theoretical curves of growth for CN lines (Aoki & Tsuji 1997) in the range from 3 to 6 km s^{-1}. Abundances for HD 112869 have been calculated using methods of high-resolution spectroscopy by Tsuji et al. (1991); Kipper (1992); Aoki & Tsuji (1997), however, the results are contradictory (see discussion in Section 3.3.12). HD 112869 exhibits semiregular light variations (SRB) with an amplitude of about 0.5 mag in the visual band (Samus et al. 2009) and a period of about 105 days was suspected. Five radial velocities measurements by R.F.Griffin revealed velocity variations in the range from –132.6 to –136.9 km s^{-1} (Yoss & Griffin 1997). Mass transfer from an AGB companion star in a binary system (Kipper 1992) or evolution of a single star on the AGB (Tsuji et al. 1991; Aoki & Tsuji 1997) are proposed to explain the observed properties of HD 112869. The basic

data for HD 112869 and the comparison stars, available in the literature, are summarized in Table 1.

In this paper the results of contemporaneous radial velocity monitoring and broadband BVR_C photometry for HD 112869 are presented. The observations are analyzed to clarify the character of variability and to search for its period. New high resolution optical spectrum was observed and analyzed using qualitative and quantitative methods relative to the comparison stars: well known N-type carbon star HD 92055 and J -type carbon star HD 25408 with enhanced ^{13}C isotopic abundance. Abundances were calculated for carbon, nitrogen, magnesium, iron, and selected neutron-capture elements, using the method of spectral synthesis and new self-consistent atmospheric models. The evolutionary status of HD 112869 is discussed.

2. Observations and data reduction

Radial-velocity monitoring of HD 112869 was started in 2006 using the CORAVEL spectrometer of the Vilnius University installed on the 1.65-m telescope at the Molėtai Observatory (Lithuania). The CORAVEL spectrometer (Upgren et al. 2002) is based on principles of the photoelectric radial-velocity scanner developed by R.F.Griffin (Griffin 1967) and it operates by scanning the spectrum of a star across the mask and obtaining an on-line cross-correlation velocity. 97 measurements are gathered for HD 112869 during about 8 years of monitoring. The standard deviation of a single observation for late-type stars brighter than about 11th magnitude is usually better than 0.8 km s^{-1}. The velocities have been standardized using the observations of IAU radial velocity standards (Udry et al. 1999) and are close to the system of velocities published by Nidever et al. (2002) and Marcy et al. (1989). The difference in zero point was found to be 0.14 km s^{-1} for F-G-K type stars and 0.4 km s^{-1} for M-type stars and exhibits rms scatters of 0.5 and 0.8 kms^{-1}, respectively.

Photometric $BVR_{\rm C}$ observations were performed from 2013 February to 2014 June at the Molėtai Observatory using the twin-telescope photometric system. It consists of the 63-cm and 25-cm telescopes for simultaneous measurements of a target star and of a comparison star, respectively, and is equipped with two identical photoelectric (multi-alkali photocathodes of type S20) photometers connected to the same data acquisition system. The ratio of counting efficiency of one telescope to that of another was checked from time to time by measuring the same star. The comparison stars, HD 114036 and HD 114357, are chosen to lie within 2° from HD 112869 and are bright enough to be accessible with the 25-cm telescope. The simultaneous measurements and the proximity of the comparison stars to HD 112869 reduced the effects of variations of atmospheric transparency.

A set of 12 standard stars of spectral types from late F to K5 was observed repeatedly at various air masses to measure atmospheric extinction and to place the data of differential photometry on a standard magnitude scale. Both the extinction coefficients and the transformation to the standard Johnson-Cousins system were then calculated using a least-squares routine which solves simultaneously all repeated observations. Since the primary standards in the Cousins system (Landolt 1992) are not accessible from the Molėtai Observatory sky, for the transformation of instrumental R_C magnitude we addressed the Catalog of $WBVR$ magnitudes of bright stars of the northern sky by Kornilov et al. (1991), in which all of these 12 standard stars are found. The R magnitude of the $WBVR$ catalog, however, is not in the Cousins system, therefore we transformed it to $R_{\rm C}$ using an additional set of 19 stars having both the Cousins and $WBVR$ photometry. The uncertainty of the transformation equation obtained for R is 0.018 mag. Standardized $BVR_{\rm C}$ photometry of the comparison stars is listed in Table 2. The bottom line of the table gives an overall error in each magnitude, estimated taking into account both the measurement error and the transformation uncertainties. These stars should serve as useful comparison objects for photometric monitoring of HD 112869 in the future.

The high-resolution spectra for HD 112869 and for the spectroscopic comparison stars HD 92055 and HD 25408 were observed with the coudé échelle spectrometer MAESTRO fed by the 2-m telescope at the Observatory on the Terskol Peak in Northern Caucasus, equipped with a CCD detector and having a resolving power of ∼45 000. The spectrum of HD 112869 was observed during an exposure of 7200 s with S/N ratio of about 80 near H_α on the night of 2013 March 8. The spectra of both comparison stars are retriewed from the MAESTRO archive of high resolution spectra. These observations were carried out in 2001 January and 2003 February, respectively. All the employed spectra cover the wavelength region from about 3600 to 9300 Å in 85 wavelength bands overlapping in the red and near infrared wavelengths regions. All the spectra were bias subtracted, flat-field corrected, and converted to one-dimensional spectra using the standard DECH20T package.[1] The wavelength calibration was made using Th−Ar and sky spectra obtained for each night. In addition, a spectrum of a hot and rapidly rotating star was observed to identify the telluric absorption lines. Two representative wavelength regions for HD 112869, along with those for the comparison stars, are shown in Figures 1 and 2.

[1]http://www.gazinur.com/Spectra-Processing.html

Table 1: The basic data for HD 112869 and spectroscopic comparison stars collected from literature.

HD	Name	Sp.Type	M_{bol}	T_{eff}	[Fe/H]	C/O	$^{12}C/^{13}C$	[s/Fe][a]	[hs/ls][b]	Ref
112869	TT CVn	C 4,5 CH	-3.35	3700	-2.9	1.07	50-90	+2.5	+0.8	1
				3700	$\approx$ -2.0	6.3	$\geqslant$500	...	...	2
25408	UV Cam	C 5,3 CH	-4.85	3000	-0.82	1.20	5	+1.2	+0.7	3
			-8.70	3350	+0.2[c]	...	4	+0.09[d]	...	4
92055	U Hya	C 6,3	-4.0	2825	-0.05	1.05	35	+1.0	0.0	5

[a] s = <ls + hs >

[b] hs = <Ba, La, Ce, Nd, Sm>, ls = <Sr, Y, Zr>

[c] mean metallicity: [M/H]

[d] [s/M]

References. — (1) Kipper (1992); (2) Aoki & Tsuji (1997); (3) Kipper et al. (1996); (4) Abia & Isern (2000); (5) Abia et al. (2002)

Table 2: Estimated magnitudes and overall errors for the photometric comparison stars.

Star	Sp.Type	B (mag)	V (mag)	R_C (mag)
HD 114036	G8 V	9.010	8.153	7.587
HD 114357	K2 III	7.247	6.014	5.270
Error		0.018	0.015	0.024

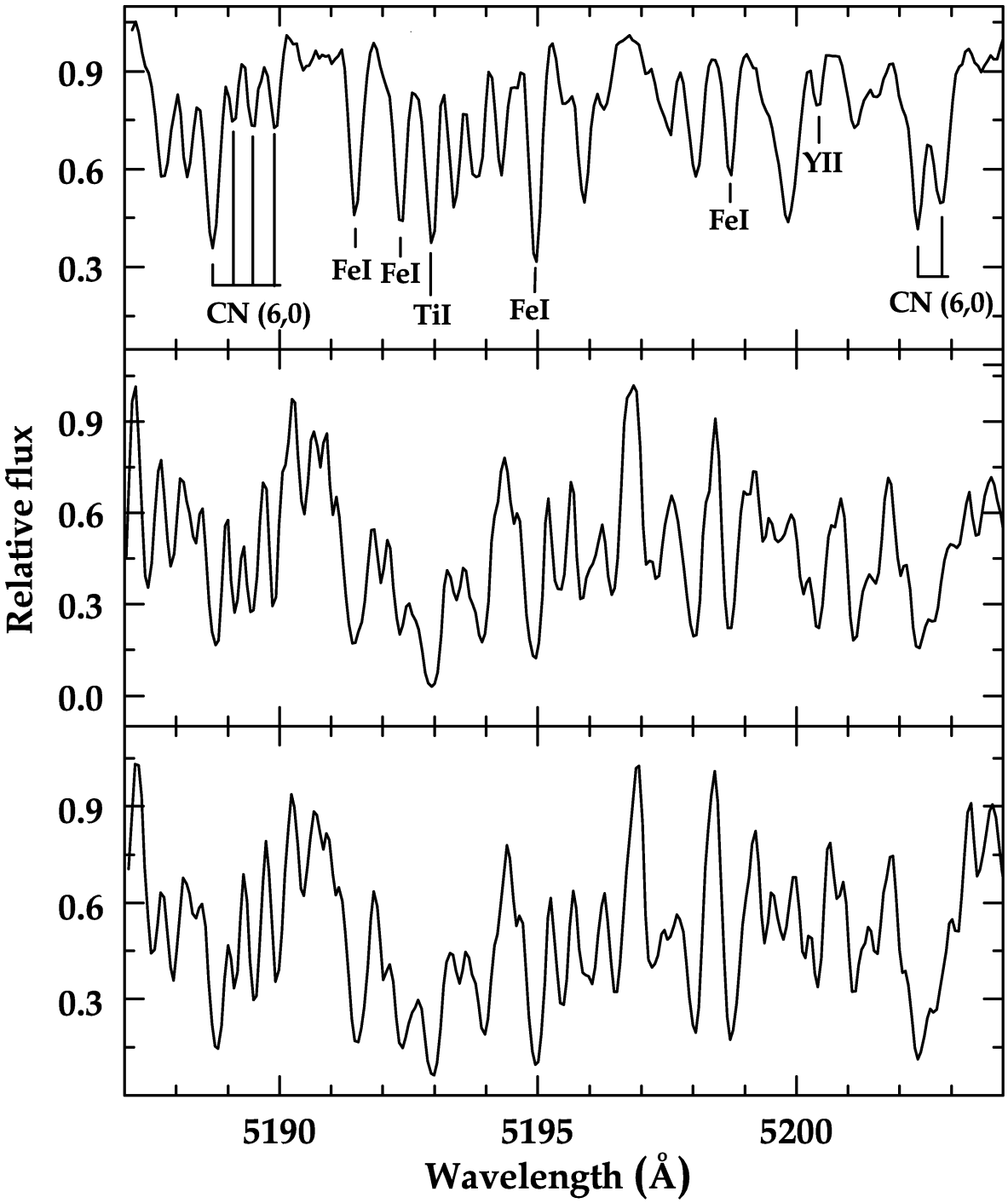

Fig. 1.— Spectrum of HD 112869 (top panel), along with that for the comparison stars HD 92055 (middle panel) and HD 25408 (bottom panel), in the spectral region less blended by molecular features. Iron and yttrium lines are relatively weak in the spectrum of HD 112869 in comparison with those for the comparison stars.

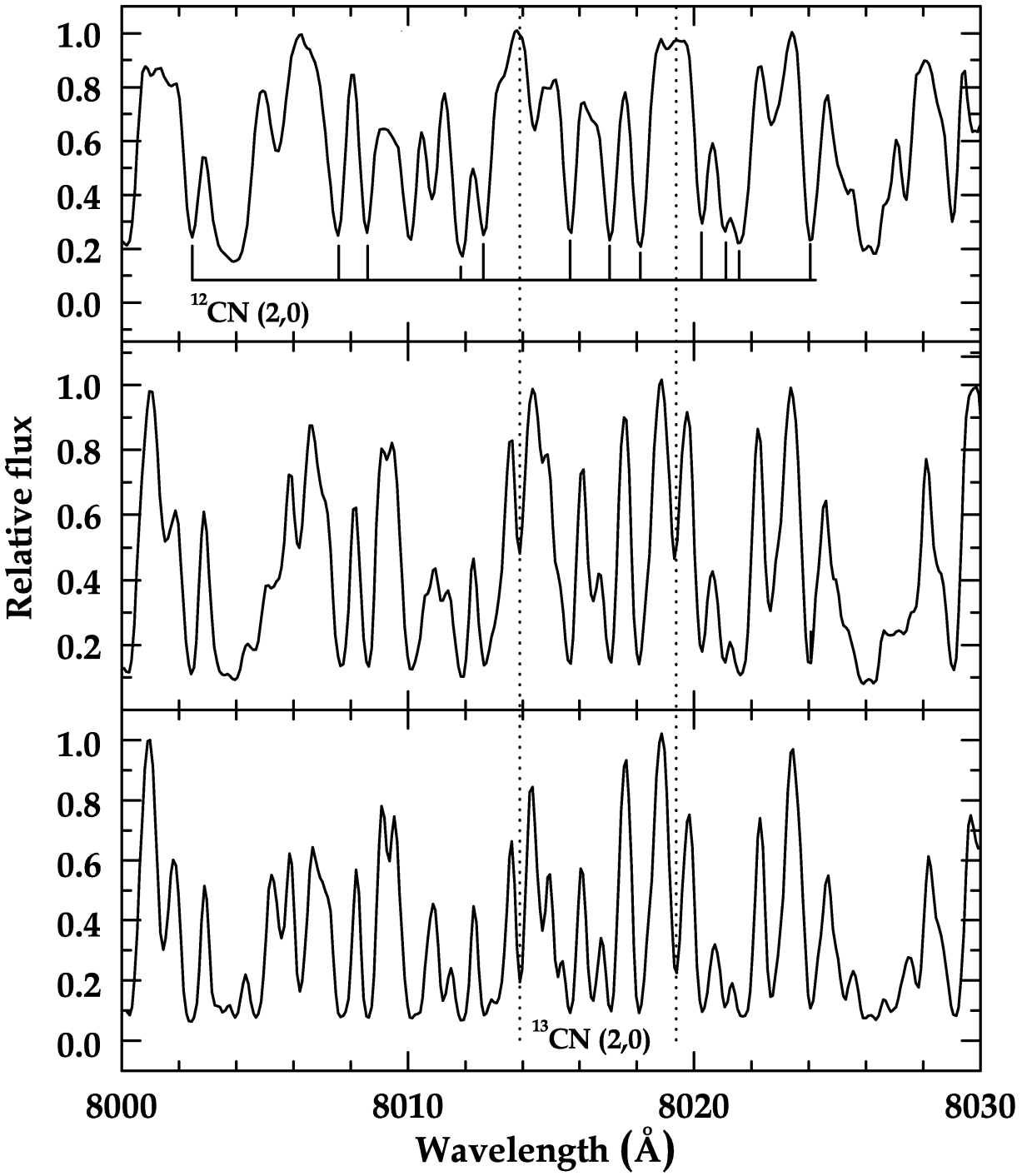

Fig. 2.— Same as Fig. 1, but in the region of selected CN(2,0) lines. The isotopic ^{13}CN lines are not clearly visible in the spectrum of HD 112869. Thus a high $^{12}C/^{13}C$ ratio is confirmed in comparison with that of HD 92055 ($^{12}C/^{13}C = 35$) and HD 25408 ($^{12}C/^{13}C = 4$).

3. Analysis and results

3.1. Radial velocities

Heliocentric radial velocities ($RV_{\odot}$) for HD 112869 as a function of Heliocentric Julian Date (HJD), measured using the CORAVEL spectrometer, are listed in Table 3, along with the uncertainty of each observation. The radial velocity curve is shown in Figure 3. As can be seen, a variation in the radial velocities reaches about 10 km s^{-1}. A periodogram analysis was carried out of the radial velocity data set of 97 data points and a significant period was detected, P = 114.9 days. However, the character of variability varies from cycle to cycle. During the time span HJD 2454850-5050 the variations are quite regular, however, recent radial velocity data display a significant deviation from a sine wave (see Figures 3 and 4). It can be seen also that the scatter of velocities near the velocity extremums sometimes exceeds remarkably the error of measurements and such a large scatter probably reflects some physical processes in the atmosphere/envelope of the star. All the velocity measurements for HD 112869, as a function of phase, resulting from the approximation by a sine wave with a period of 114.9 days, are plotted in Figure 5 (top panel). The radial-velocity monitoring shows with certainty that HD 112869 is a pulsator with a dominating pulsation period of about 115 days and a variability pattern typical of the evolved low mass stars (see Hrivnak et al. (2013) and references therein).

3.2. Photometry

The results of BVR_C photometry are given in Table 4. The columns contain the following information: time of the measurement, the mean magnitude V and color indices (B-V) and (V-R_C) averaged over each night, and the corresponding standard errors. It should be noted that the errors given are photometric uncertainties and reflect primarily the actual observing conditions. The light curves show a cyclical variations with amplitudes of ∼0.84 mag in B, ∼0.71 mag in V, and ∼0.66 mag in R_C. The light variations in V band are shown in Figure 4, along with the velocity measurements during the last observed cycle of pulsations. A large scatter in the velocities ($\sim 6\sigma$) near HJD 2456680 and a significant departure from a sine wave in the V light are clearly seen. All the photometric data phased with a period of 114.9 days are given in Figure 5. As it can be seen, the dominating period of pulsations calculated using photometry is close to that found on the basis of radial velocities. The light variations are accompanied by color variations what lends observational support to the stellar pulsations (Figures 4 and 5). The color curves mimic the cyclical variations in the light curve, with the star seen to be redder when it becomes fainter. A comparison of the

Table 3: CORAVEL radial-velocity measurements for HD 112869 along with the uncertainties.

HJD -2,450,000	$RV_\odot$ (km s^{-1})	σ (km s^{-1})	HJD	$RV_\odot$	σ	HJD	$RV_\odot$	σ
3867.361	-133.8	0.9	5301.544	-130.1	0.7	6676.590	-129.0	0.8
3889.428	-132.7	0.8	5302.50	-129.8	0.8	6677.617	-129.3	1.0
3899.386	-132.0	0.8	5346.366	-135.5	0.5	6679.660	-129.3	0.8
4244.423	-132.9	1.1	5352.346	-135.4	0.6	6680.646	-130.6	0.7
4245.397	-132.0	0.7	5365.371	-135.4	0.8	6681.639	-128.4	0.8
4581.453	-136.4	0.5	5366.350	-135.4	0.5	6682.686	-131.0	0.7
4582.417	-135.8	0.5	5875.691	-130.9	0.7	6683.582	-129.2	0.6
4864.573	-132.1	0.7	5881.665	-130.6	0.9	6683.609	-129.4	0.8
4864.591	-132.5	0.6	5967.573	-134.2	0.7	6687.586	-132.0	0.8
4865.582	-132.2	0.7	5968.611	-134.3	0.5	6693.594	-127.9	0.7
4916.475	-135.9	0.5	5974.617	-134.4	0.7	6694.600	-127.1	1.0
4929.381	-134.7	0.5	5994.551	-131.2	0.7	6713.533	-134.0	0.6
4930.295	-133.9	0.6	5995.473	-131.7	0.6	6727.511	-133.5	0.6
4940.435	-132.8	0.6	6000.476	-130.4	0.7	6727.523	-134.3	0.6
4941.472	-132.4	0.5	6010.550	-131.8	0.6	6728.483	-135.6	0.7
4942.413	-133.0	0.5	6023.407	-135.2	0.6	6737.497	-133.0	1.2
4944.348	-132.6	0.7	6035.422	-137.3	0.6	6737.572	-134.8	1.5
4946.393	-132.1	0.6	6071.427	-136.0	0.7	6752.453	-136.3	0.5
4947.389	-132.0	0.5	6072.375	-134.8	0.8	6758.379	-136.4	0.5
4950.401	-131.8	0.5	6086.444	-131.1	0.8	6758.409	-135.6	0.5
4953.422	-131.8	0.6	6315.595	-132.5	0.7	6764.396	-133.8	0.6
4967.516	-131.6	0.7	6317.569	-132.0	0.7	6770.372	-134.2	0.7
4968.325	-131.3	0.6	6325.433	-132.6	0.8	6770.468	-133.2	0.5
4968.332	-131.5	0.6	6349.447	-131.7	0.7	6773.384	-133.3	0.5
5000.378	-134.6	0.6	6359.414	-130.5	0.5	6776.394	-131.6	0.5
5013.371	-136.0	0.6	6374.471	-133.4	0.7	6782.360	-131.0	0.8
5027.345	-136.2	0.5	6379.454	-134.3	0.7	6792.431	-128.8	0.6
5030.348	-135.7	0.5	6389.552	-136.1	0.6	6799.344	-127.1	0.5
5030.368	-135.5	0.6	6391.497	-135.8	0.8	6800.511	-127.9	0.8
5037.384	-134.0	0.7	6398.373	-133.9	0.6	6819.376	-133.3	0.7
5220.668	-133.4	0.6	6399.435	-134.2	0.7	6821.370	-133.2	0.7
5266.505	-136.3	0.6	6404.398	-133.8	0.7	...	...	...
5278.481	-134.3	0.5	6614.668	-136.8	0.7	...	...	...

light, color, and velocity curves reveals that the light and color curves are about in phase, while the radial velocity curve is out of phase with the light curve. Thus, the radial velocity and light/color variations display the correlations observed for the pulsating evolved stars (see Hrivnak et al. (2013); and references therein).

3.3. High-resolution spectroscopy

3.3.1. Description of spectrum and line selection.

Strong absorption lines of carbon bearing molecules are dominating the spectrum of HD 112869. The most prominent molecular features in the optical wavelength region are the C_2 Swan system band heads (0,0) at 5165 Å, (1,0) at 4740 Å, and (0,1) at 5635 Å (see Figure 6). In addition, over the entire analyzed wavelength region, strong lines of CN and CH molecules are evident, blending significantly the atomic absorption lines. However, in some wavelength regions, contamination from molecules is lower, e.g. redward of the Swan system bandheads. A qualitative inspection of the observed high-resolution spectrum for HD 112869 shows that, relative to the comparison stars, lines of the iron-peak and neutron-capture elements are much weaker and molecular lines with isotopic ^{13}C are not clearly visible (e.g. Figures 1 and 2). The selection of relatively unblended atomic lines for abundance analysis was done using the synthesized molecular spectra over all the wavelength region employed.

3.3.2. Atmospheric models

The first iteration of abundance analysis was carried out using the atmospheric model calculated by T.Kipper with the code SCMARCS 21.1 for the published atmospheric parameters and abundances: $T_{eff} = 3700$ K, $\log g = 0.4$ (cgs), $\xi_t = 4.0$ km s^{-1}, [Fe/H] $= -3.0$, and $C/O = 1.07$ (Kipper 1992). The next iterations were made using two atmospheric models calculated by U.G.Jørgensen for $T_{eff} = 3800$ K and a high carbon to oxygen ratio, $C/O =$ 2.5 and 26.3. The final atmospheric model was calculated using the code SAM12, a modification of Kurucz's code ATLAS12 (Kurucz 2005), produced to calculate the atmospheric models of red giants of a given chemical composition (Pavlenko 2003). The bound−free absorption caused by the C I, N I, and O I atoms was added (Pavlenko & Zhukovskaya 2003) to the continuum absorption sources included in ATLAS12. We also take into account the CIA (Collision Induced Absorption) – absorption of the molecular complexes He$-H_2$ and H_2-H_2 induced by collisions which becomes an important source of opacity in the atmospheres of cool metal-poor stars (Borysow et al. 1997). Molecular and atomic absorption in SAM12 is

Table 4: BVR_C photometry for HD 112869 along with the standard deviations.

HJD	V	σ_V	$B-V$	$\sigma_{(B-V)}$	$V-R_C$	$\sigma_{(V-R_C)}$
−2,450,000	(mag)	(mag)	(mag)	(mag)	(mag)	(mag)
6349.427	9.182	0.005	1.652	0.011	0.896	0.009
6359.439	9.179	0.007	1.661	0.008	0.913	0.008
6369.445	9.042	0.004	1.630	0.008	0.908	0.013
6379.436	8.920	0.010	1.635	0.014	0.880	0.014
6391.557	8.958	0.006	1.621	0.008	0.900	0.009
6398.401	9.027	0.014	1.623	0.017	0.903	0.018
6399.380	9.021	0.011	1.643	0.012	0.882	0.012
6404.374	9.078	0.004	1.639	0.006	0.898	0.008
6418.403	9.132	0.006	1.641	0.007	0.898	0.017
6694.613	9.150	0.008	1.808	0.014	0.933	0.010
6713.615	8.862	0.011	1.694	0.021	0.897	0.012
6727.471	8.944	0.011	1.654	0.021	0.880	0.012
6737.508	9.019	0.004	1.660	0.007	0.883	0.010
6745.475	9.088	0.002	1.676	0.009	0.884	0.005
6758.373	9.114	0.008	1.676	0.012	0.880	0.013
6764.420	9.160	0.015	1.689	0.017	0.887	0.015
6771.433	9.304	0.004	1.699	0.015	0.909	0.007
6776.390	9.414	0.002	1.717	0.005	0.920	0.009
6782.383	9.573	0.014	1.823	0.024	0.950	0.020
6792.497	9.511	0.027	...	...	0.898	0.028
6799.382	9.413	0.003	1.811	0.022	0.912	0.008
6800.378	9.390	0.018	...	...	0.924	0.022
6804.441	9.213	0.009	...	...	0.863	0.051
6814.437	8.961	0.002	1.687	0.013	0.889	0.021

taken into account by using the opacity sampling technique (Sneen et al. 1976). A compiled list of spectral lines includes the atomic lines from the VALD database (Piskunov et al. 1995; Kupka et al. 1999) and the molecular lines CN, C_2, CO, SiH, MgH, NH, OH from the Kurucz database (Kurucz 1993). In addition, the absorption by the HCN bands was taken into account according to Harris et al. (2003, 2006). We took into account also the absorption of the isomers HCN and NHC. The atmospheric model was calculated for the accepted atmospheric parameters, [Fe/H], and $\log(C/O)$. The model abundances were corrected according to the actual chemical composition calculated for the HD 112869 atmosphere during the subsequent iterations. We adopted a high $^{12}C/^{13}C = 500$ ratio in the calculations of the final atmospheric model. A temperature structure of the atmospheric models for carbon giants is less sensitive to $^{12}C/^{13}C$ (Pavlenko 2003). The temperature structure of the final set of atmospheric models is shown in Figure 7.

3.3.3. Atmospheric parameters

We adopted an effective temperature of 3900 K for the final atmospheric model, which is a mean value estimated using IRFM by three authors (see Section 1). The use of ionization balance for the calculation of surface gravity seems to be problematic because of significant effects of nonlocal thermodynamic equilibrium (NLTE) for iron (see Section 3.3.5). We find $\log g$ lower than zero, if we estimate the gravity by assuming LTE and requiring the iron abundances derived by analysis of Fe I and Fe II lines to be equal, which contradicts the value of g calculated for $M_{bol} = -3.35$ mag assuming for HD 112869 a mass of $1M_{\odot}$, log g = 0.4 (cgs). The microturbulent velocity was determined by forcing the abundances of individual lines to be independent of the equivalent width. The final atmospheric parameters used for abundance analysis are (T_{eff}, $\log g$, ξ_t) = (3900 K, 0.4 (cgs), 4.0 km s^{-1}). Notice that the adopted values of effective temperature and surface gravity are in line with the overall relationship established for CEMP stars (see Figure 1 in Bisterzo et al. (2011).

3.3.4. Spectral synthesis

The abundances of carbon, nitrogen, and the ratio of carbon isotopes are estimated by synthesis of C_2 and CN spectra around the bandheads of Swan, Phillips, and CN Red systems in a broad wavelength region from about 4700 to 9000 Å, using a standard technique adopted for the analysis of cool carbon-rich stars (see, for instance, Zamora et el. (2009)). We concluded during the subsequent iterations that the calculated C_2 and CN spectra reproduced the observed molecular features quite well near the bandheads despite

of the star's complicated spectrum. The abundances for other than carbon and nitrogen elements are calculated by synthesis of the profiles of less blended atomic lines (see Table 5), apart from strong bandheads where the number and intensity of molecular lines is lower. Unfortunately, the fit between the calculated and observed molecular spectrum for the final C and N abundances becomes worse apart from the molecular bandheads because of increased uncertainties of molecular data, especially for the C_2 Swan system. Therefore, calculation of the abundances using atomic lines is a challenge for cool carbon-rich stars. Weak atomic lines are detectable far from molecular bandheads where a correct estimation of molecular contribution is plagued due to lower quality of molecular data. In the case of poor reproduction of the observed molecular spectrum in the surroundings of selected atomic lines for the final C and N abundances, only synthesized atomic spectra were fitted to the observed spectrum and, in this way, an upper limit of abundance was derived (see Table 6).

The synthetic spectra are calculated withs the code WITA (Pavlenko 1997) and are convolved with the instrumental profile, for which we used a Gaussian with FWHM from ∼0.20 to 0.30 Å depending on the wavelength region. The system of continuum opacity sources was used the same as for the model atmospheres calculations. As a primary source of atomic data the VALD database was used. The list of molecular lines was adopted from the Kurucz database (Kurucz 1993) and SCAN tape (Jørgensen & Larsson 1990). The mean absolute and relative abundances, calculated using the final model and the adopted atmospheric parameters, are given in Table 6, together with the internal random error (σ), calculated by a root mean squere method, and the number of lines (n) used in the analysis. The standard notations are adopted everywhere.[2] The resulting relative abundances normalized by the solar-system abundances are calculated using the chemical composition for the solar photosphere provided by Asplund et al. (2009). Figures 8−21 illustrate synthesis of representative wavelength regions and atomic lines.

The systematic errors in the abundances, produced by uncertainties in T_{eff} (±200 K), $\log g$ (±0.3 dex), and ξ_t (±0.5 km s^{-1}), would lead to errors less than 0.3 dex (except for nitrogen). The uncertainty in the continuum normalization was estimated to be within 2% over the most of the wavelenght regions employed. The atmosphere of HD 112869 is warmer and the spectrum is less crowded in comparison with those observed for N type carbon stars. In most of the modelled regions the S/N ratio is high and the continuum was clearly identified in the spectrum. The synthesized atomic and molecular spectra helped us to define short wavelength regions in the spectrum which are free of absoption lines. The spectrum was normalized using a low-order polynomial fit to the selected regions. In the

[2][A/B] = $\log (N_A/N_B)_\star$ - $\log (N_A/N_B)_\odot$, where N_A, N_B is the number density of an element A and B. $\log \epsilon(A) = \log (N_A/N_H) + 12.00$, where N_H is the number density of hydrogen.

case of doubt, some of the regions were omitted and the rest ones were fitted again with the goal to examine the uncertainty of normalization. On the other hand, the carbon abundance was calculated using C_2 lines in the broad wavelength region from about 4700 to 9000 Å (see Section 3.3.6). We have not found any trend of the calculated carbon abundance from the wavelength of employed region, $log\,\epsilon(C) = 8.3 \pm 0.1$ dex. Thus, the systematic error in the spectrum normalization should be relatively low. Blueward of C_2 bandheads, the uncertainty exceeds 5%, a value typical for cool carbon stars (see, for instance, Abia et al. (2002). The systematic errors in the calculated abundances ($\Delta \log \epsilon$(X)) are estimated on the basis of abundances derived using the modified atmospheric models (see Figure 7). The conclusion is that the error due to uncertainty in the adopted temperature is the largest for the nitrogen abundance and decreases for the abundances of iron peak and s-process elements: $\Delta \log \epsilon$(C) ∼0.2 dex, $\Delta \log \epsilon$(N) ∼ 0.5 dex, $\Delta \log \epsilon$(Mg) ∼0.15 dex, $\Delta \log \epsilon$(Ti) ∼0.25 dex, $\Delta \log \epsilon$(Fe) ∼0.15 dex, and $\Delta \log \epsilon$(s-process) <0.1 dex. The systematic errors due to uncertainty in the adopted gravity are larger for the abundances derived by analysis of the ionized lines. We conclude, that these errors are less than 0.1 dex. The systematic errors arising from uncertainty in the adopted microturbulent velocity are larger for the elements represented by relatively strong lines. For example, the magnesium abundance was calculated on the basis of lines with the equivalent widths between 300 and 400 mÅ. However, these systematic errors are less than ∼0.1 dex for the lines used. The systematic errors due to uncertainties in the continuum normalization are larger for the abundances derived by analysis of weak lines and these errors can reach 0.1 dex. The systematic error in the derived $^{12}C/^{13}C$ ratio, produced by an uncertainty of 2% in the continuum normalization over the wavelength region around C_2 (1,0) bandhead, was found to be ±300. The root-sum-squared (RSS) uncertainties calculated taking into account all sources of errors are less than ∼0.4 dex, what is a typical total uncertainty in abundance analysis of cool carbon stars (Zamora et el. 2009).

3.3.5. Iron

A limited number of relatively clean iron lines was selected for HD 112869. Using six Fe II lines, we calculated the star's mean metallicity, [Fe/H] = −2.3, however, the neutral lines of Fe I provide lower metallicity, [Fe/H] = −2.6 dex, on average (see Figures 8 and 9). It seems likely that neutral atomic lines suffer from NLTE effects; these are significant at low metallicity and high luminosity. Shchukina et al. (2005) have shown that for metal-poor stars the NLTE abundance corrections for Fe I can reach about 0.9 dex. As argued by many authors, Fe II lines are more reliable abundance indicators than Fe I lines, since such lines are nearly independent on the departures from NLTE and the temperature structure of model atmospheres. Thus, we conclude that the metallicity of HD 112869 is higher than estimated

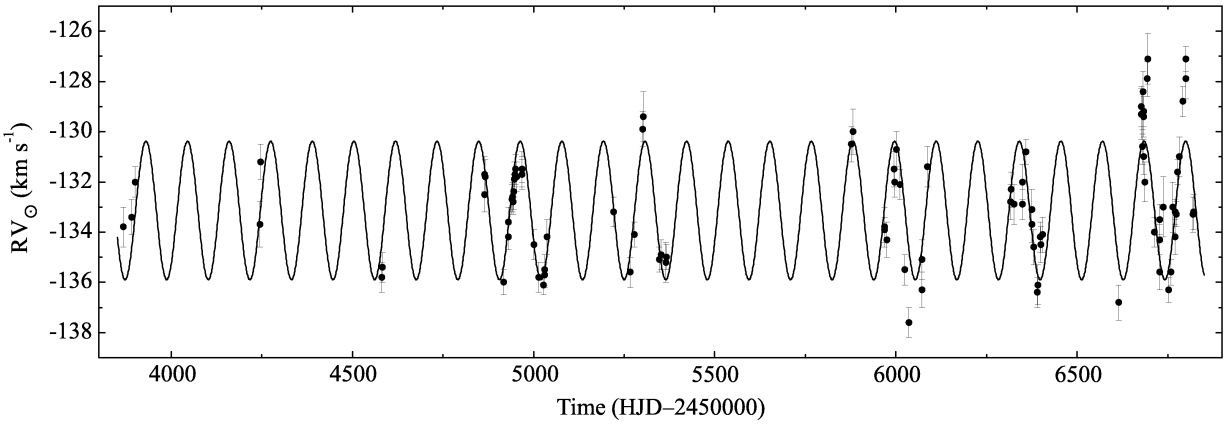

Fig. 3.— Heliocentric radial velocity of HD 112869 measured using the CORAVEL spectrometer (filled circles), illustrating a semiregular character of variability. The observations are approximed by a sine wave with a period of P = 114.9 days and an amplitude of A = 2.8 km s^{-1}.

Table 5: List of the lines for neutron-capture elements, synthesized in the spectrum of HD 112869. Wavelengths, excitation potentials, and gf-values are given.

Wavelength (Å)	Species	LEP (eV)	log(gf)
4077.709	Sr II	0.00	0.167
4086.709	La II	0.00	-0.070
4220.660	Sm II	0.544	-0.440
4900.120	Y II	1.03	-0.09
4934.076	Ba II	0.00	-0.15
5200.406	Y II	0.992	-0.57
5205.724	Y II	1.033	-0.340
5249.576	Nd II	0.976	0.200
5255.502	Nd II	0.205	-0.670
6141.713	Ba II	0.704	-0.076
6645.094	Eu II	1.380	-0.162
6645.114	Eu II	1.380	-0.200

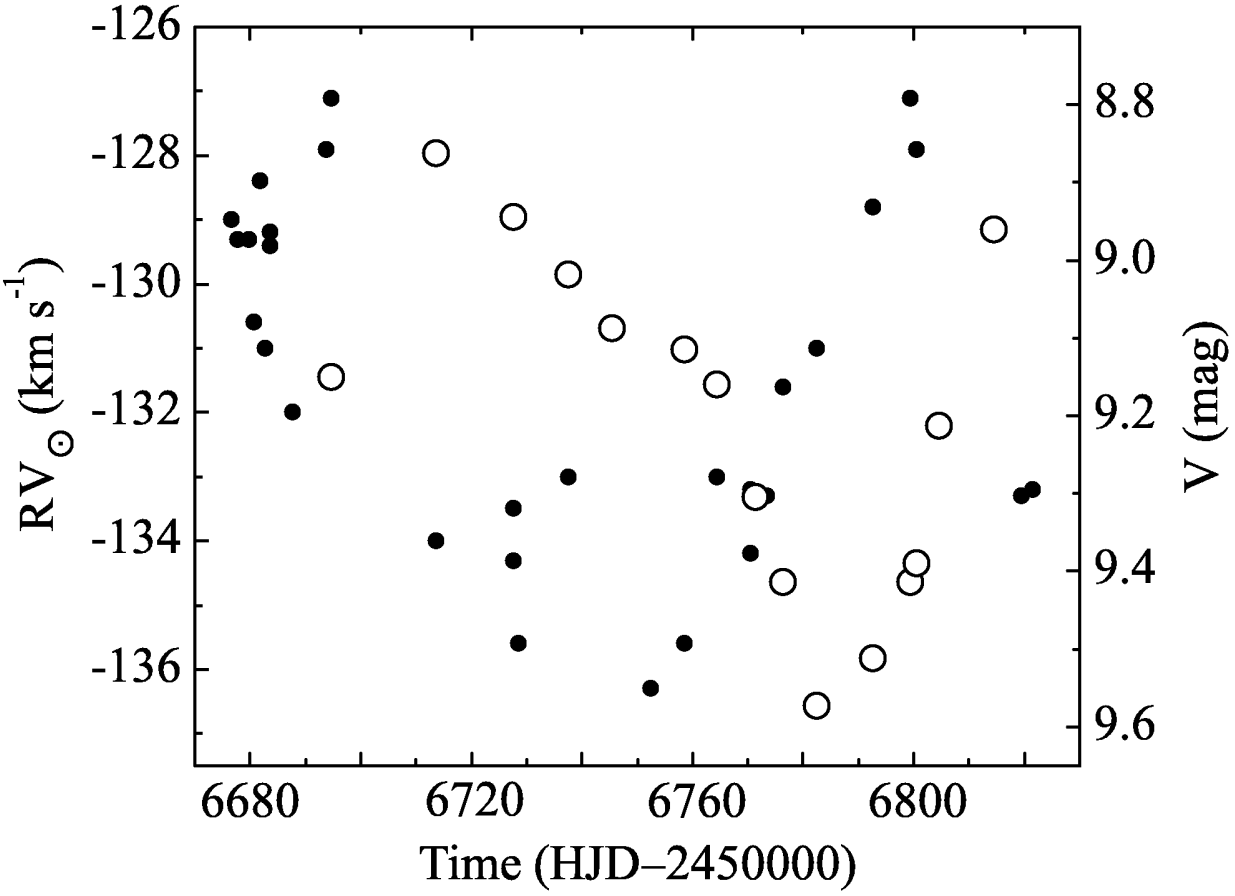

Fig. 4.— Heliocentric radial velocity of HD 112869 measured using the CORAVEL spectrometer (filled circles) along with the apparent magnitude in V band (open circles) for the last observed cycle, confirming the pulsational nature and semiregular character of the variability.

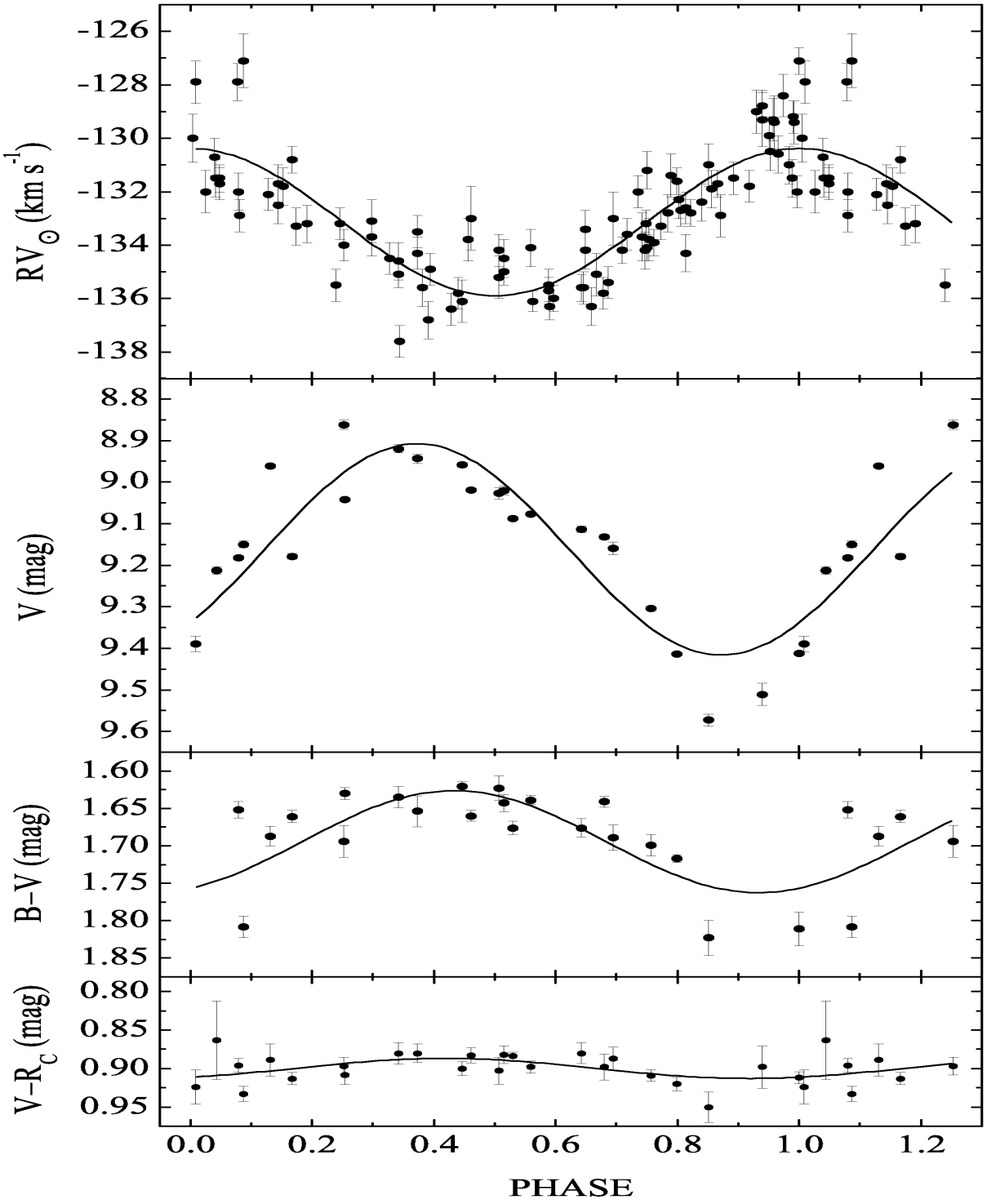

Fig. 5.— CORAVEL radial velocities (top panel) and photometry for HD 112869 phased with a period of 114.9 days. The fit with a sine wave is shown.

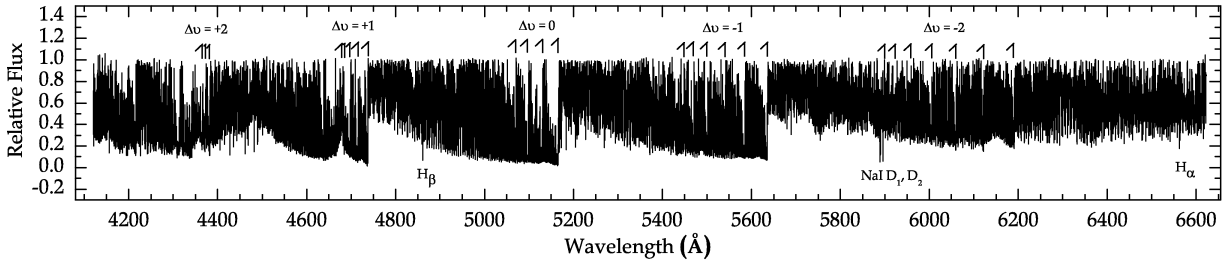

Fig. 6.— Normalized high resolution spectrum of HD 112869 in the wavelength region from 4100 to 6650 Å. The dominating C_2 Swan system $\Delta v = +2, +1, 0, -1, -2$ bandheads and a few prominent atomic lines are marked.

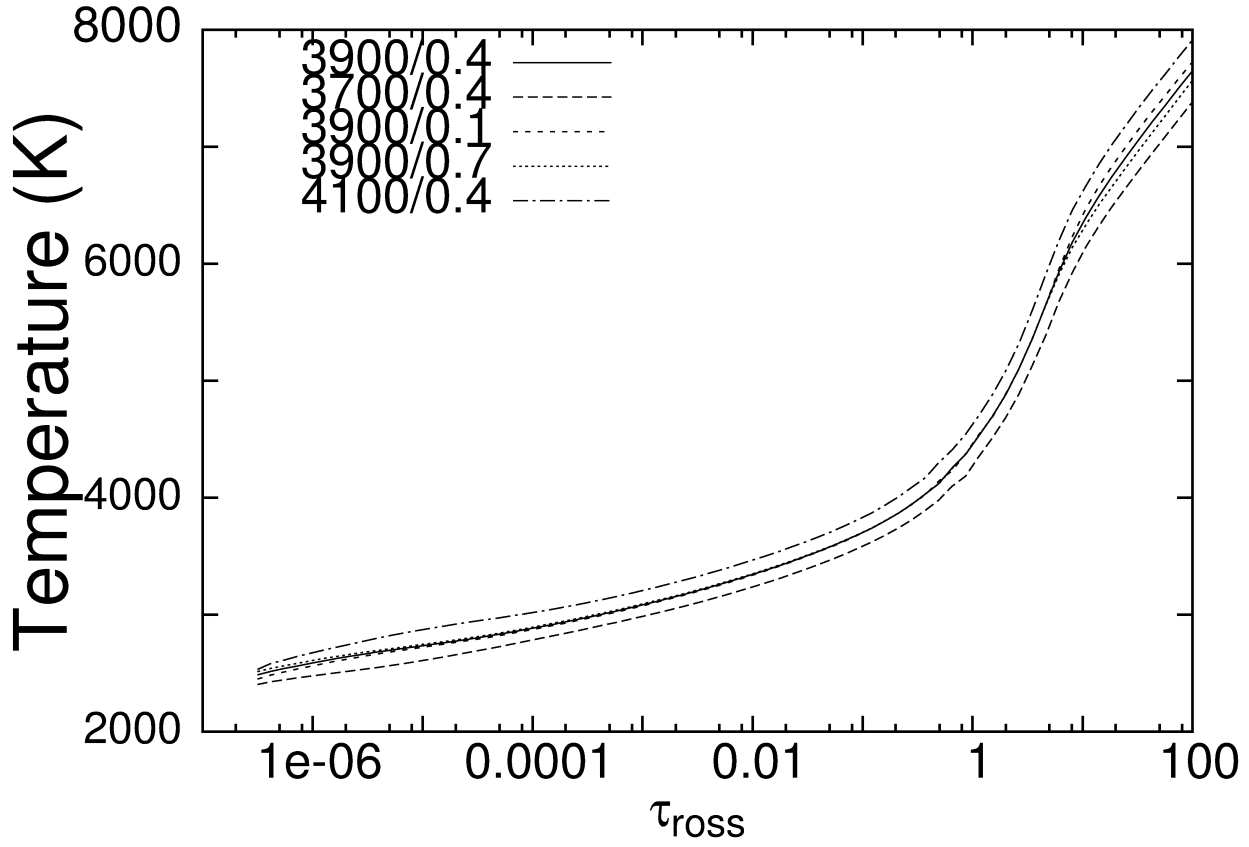

Fig. 7.— Temperature structure of the final atmospheric model calculated for HD 112869 (solid line), along with that for the modified models ($\Delta T_{\rm eff} = \pm 200$ K, $\Delta \log g = \pm 0.3$ (cgs)) used for estimation of systematic errors.

Table 6: Averaged absolute and relative abundances for HD 112869, along with the random error and the number of lines used in the synthesis.

X	$log\,\epsilon(X)$	n	σ	[X/H]	[X/Fe II]
C	8.30	C_2	0.1	-0.13	+2.17
N	6.55	CN	0.2	-1.28	+1.02
Mg I	4.6	3	0.3	-3.00	-0.7
Ti I	2.7	3	0.3	-2.23	+0.1
Ti II	3.1	2		-1.85	+0.5
Cr I	2.4	3	0.3	-3.29	-1.0
Fe I	4.9	14	0.2	-2.60	-0.3
Fe II	5.2	6	0.2	-2.30	...
Sr II	$\lesssim$ -1.1	1		$\lesssim$ -3.97	$\lesssim$-1.7
Y II	$\lesssim$ -0.1	3	0.2	$\lesssim$ -2.27	$\lesssim$ 0.0
Ba II	$\lesssim$ -0.4	2		$\lesssim$ -2.6	$\lesssim$-0.3
La II	$\lesssim$ -0.4	1		$\lesssim$-1.55	$\lesssim$+0.8
Nd II	$\lesssim$ -0.2	2		$\lesssim$ -1.67	$\lesssim$+0.7
Sm II	$\lesssim$-0.8	1		$\lesssim$ -1.80	$\lesssim$+0.5
Eu II	$\lesssim$ -1.0	1		$\lesssim$-1.52	$\lesssim$+0.8

before, [Fe/H] = -2.3 ± 0.2 dex, assuming that the lines of ions are the safest abundance indicators. However, the iron group element chromium seems to be more depleted than iron, [Cr/Fe] $\simeq -1.0$ dex, as based on neutral chromium lines. Note that the iron peak elements chromium and manganese are underabundant in most of the analyzed CEMP stars and the [Cr/Fe] ratio decreases at lowest Fe abundances (Norris et al. 2001; Allen et al. 2012).

3.3.6. Carbon

Carbon abundance was derived from the C_2 Swan and Phillips system lines synthesized in the wavelenght region from about 4736 to 6200 Å and in the near infrared. Figures 10 and 11 illustrate the fit between the observed and calculated spectrum in two wavelengths regions - around C_2 Swan system bandheads (0,0) and (1,1) shortward of 5170 Å and around Phillips system lines in the near infrared from 8830 to 8931 Å. The given synthetic spectra are generated using the final atmospheric parameters adopted for the high carbon abundance, $log\,\epsilon(C) = 8.3$. The C_2 Swan system bandheads are saturated and the sensitivity of the calculated spectra to the adopted carbon abundance near the bandheads is low. However, the sensitivity increases for weaker lines between the bandheads. In Figure 12 we illustrate the sensitivity of the calculated spectra from the adopted carbon abundance. The mean carbon abundance was found to be high in the atmosphere of HD 112869, $log\,\epsilon(C) = 8.3 \pm 0.1$ dex.

3.3.7. Nitrogen

The nitrogen abundance was calculated by spectral synthesis of CN Red system lines in the wavelength region from about 7800 to 8100 Å. The sensivity of the synthesized CN spectrum to the adopted abundance of nitrogen is lower than in the case of C_2 lines to the carbon abundance. Therefore, the uncertainty in the fitting of the synthetic CN spectrum to the observed one is larger. The best fit between the observed and synhesized spectra was found for the nitrogen abundance $log\,\epsilon(N) = 6.55$. An extract of the spectra illustrating the synthesis of CN Red system lines is shown in Figure 13.

3.3.8. $^{12}C/^{13}C$ ratio

An inspection of the spectrum of HD 112869 in wide wavelength region gives evidence that isotopic lines are too weak to be clearly detected in the crowded spectrum, therefore,

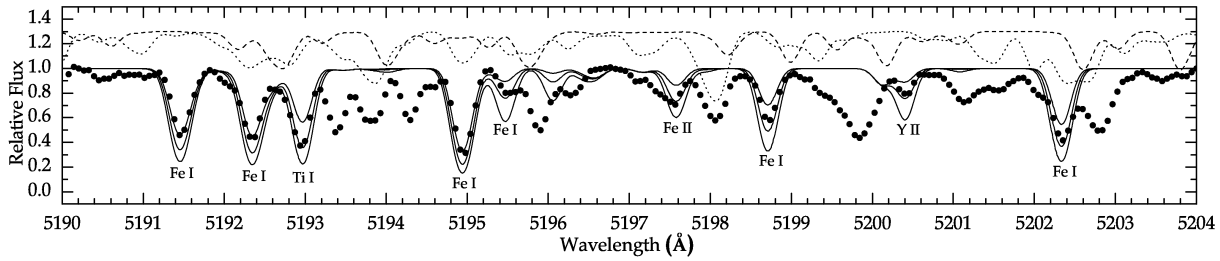

Fig. 8.— Observed spectrum of HD 112869 (filled circles), along with the synthesized atomic (solid line) and molecular (CN: dotted line; C_2: dashed line) spectra, in the wavelength region less blended by molecules, illustrating the estimation of metallicity. The synthesized profiles of atomic lines are shown for three abundances: $log\,\epsilon(Fe) = 5.2 \pm 0.5$ dex, $log\,\epsilon(Ti) = 2.7 \pm 0.5$ dex, and $log\,\epsilon(Y) = -0.1 \pm 0.5$ dex. Synthesized molecular spectra are calculated for the final carbon and nitrogen abundances.

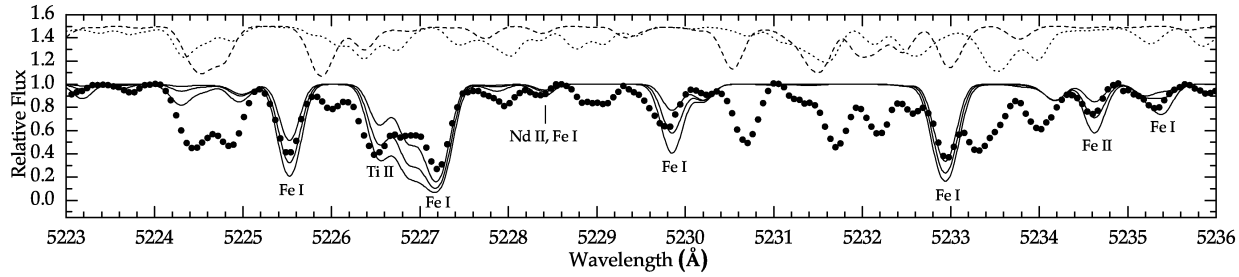

Fig. 9.— Same as Fig. 8, but in other spectral region.

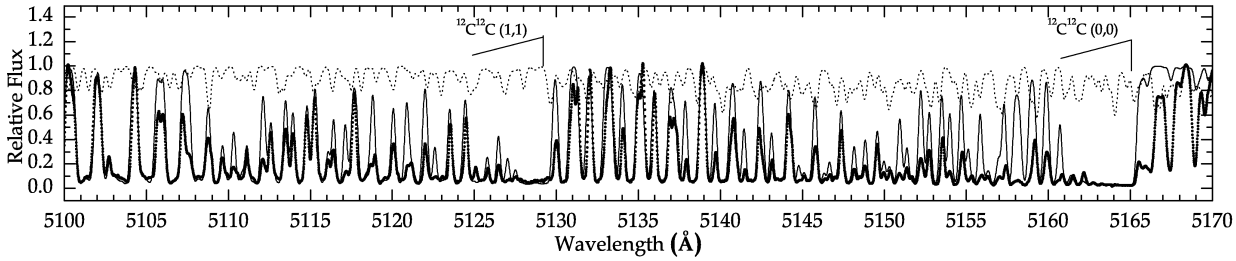

Fig. 10.— The observed spectrum of HD 112869 (solid dots), along with synthesized C_2 (solid line) and CN (dotted line) spectra, in the wavelength region dominated by Swan system $\Delta v = 0$ lines. The calculated spectra are shown for the final abundances, $log\,\epsilon(C) = 8.3$ and $log\,\epsilon(N) = 6.55$.

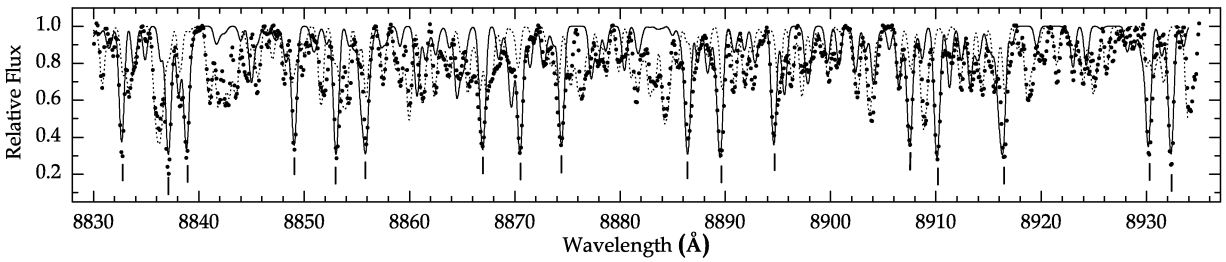

Fig. 11.— Same as Fig. 10, but in the wavelength region dominated by C_2 Phillips system lines. The synthesized C_2 and CN spectra are shown for the final abundances.

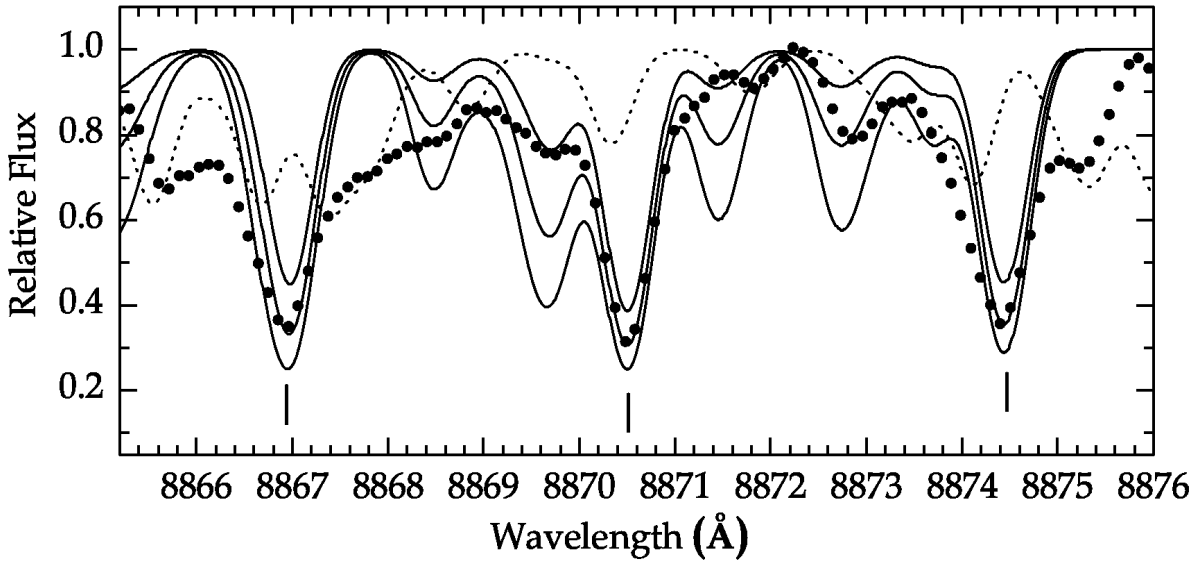

Fig. 12.— The observed spectrum of HD 112869 (filled circles), along with synthesized C_2 (solid line) and CN (dotted line) spectra, in the wavelength region dominated by Phillips system lines, illustrating the uncertainty in the derived carbon abundance. The synthesized C_2 spectra are given for three carbon abundances, $log\,\epsilon(C) = 8.3 \pm 0.2$ dex. The synthesized CN spectra are shown for the final C and N abundances.

only the lower limit of $^{12}C/^{13}C$ ratio can be determined. The C_2 (1,0) isotopic bandheads at 4744 and 4752 Å synthesized for $log\,\epsilon(C) = 8.30$ and three isotopic ratios, $^{12}C/^{13}C = 90$, 500, and 1500, are given in Figure 14. Moderatelly strong features of unknown nature, observed by Aoki & Tsuji (1997) in the wavelength region between 4738 and 4754 Å, were identified by CH lines, however, the synthesized CH spectrum is too strong for the final carbon abundance. Overestimated oscillator strengths are suspected. CH lines are blending significantly the $^{13}C^{13}C$ (1,0) bandhead, therefore, the $^{12}C/^{13}C$ limit was set using the $^{12}C^{13}C$ (1,0) bandhead. We conclude, that the isotopic ratio is extremely high in the atmosphere of HD 112869, $^{12}C/^{13}C \gtrsim 1500$. In addition, the isotopic lines of CN Red system are examined in the wavelength region from 7800 to 8100 Å. We selected less crowded wavelength regions with a certain continuum definition to estimate a reliable limit for the isotopic ratio. The results of spectral synthesis in one narrow wavelength region for three isotopic ratios are shown in Figure 15. The isotopic ^{13}CN lines are not detected certainly in the spectrum of HD 112869, in agreement with the extremely high over 500 isotopic ratio.

3.3.9. Oxygen

Spectroscopic estimation of the oxygen abundance in the optical wavelength region remains a challenge for cool carbon-rich stars. The most reliable oxygen abundances come from the forbidden [OI] line at 6300 Å. However, this line should be quite weak at low temperature and metallicity. Most of the previous high-resolution calculations of oxygen for CEMP stars were based on measurements of the lines of infrared triplet at 7771.94, 7774.17, and 7775.39 Å, which are strongly affected by NLTE effects (Asplund 2005). We synthesized the spectral region around the infrared triplet using the final atmospheric model for three oxygen abundances, $log\,\epsilon(O) = 0.0$, 6.7, and 8.7 dex. The conclusion is that at the position of the infrared triplet dominate CN lines. The oxygen lines are too weak to be detected in the spectrum of HD 112869 even for the solar abundance. Therefore, we adopted for HD 112869 the oxygen abundance $log\,\epsilon(O) = 7.2$ dex according to the relationships [O/Fe] vs. [Fe/H] (Aoki et al. 2004) and [O/Fe] vs. [C/Fe] (Kennedy et al. 2011) observed for CEMP stars : [O/Fe] $\simeq +0.8$ for [Fe/H] $= -2.3$ dex.

3.3.10. Magnesium

Magnesium is a key element for examination of α-process nucleosynthesis in the Galaxy and Mg/Fe ratio carries information about the initial mass function. The Mg I b triplet is located redward of the C_2 (0,0) Swan system bandhead at 5165 Å in the wavelenghts

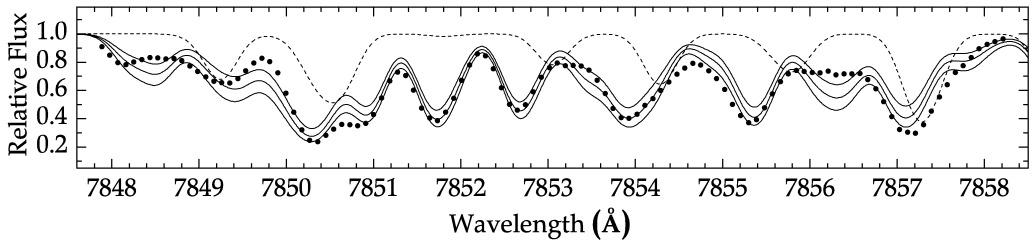

Fig. 13.— The observed spectrum of HD 112869 (filled circles), along with synthesized CN (solid line) and C_2 (dashed line) spectra, in the wavelength region dominated by CN Red system lines, illustrating the uncertainty in the derived nitrogen abundance. The synthesized CN spectra are given for three nitrogen abundances, $log\,\epsilon(N) = 6.55 \pm 0.2$ dex. The adopted carbon abundance is $log\,\epsilon(C) = 8.3$.

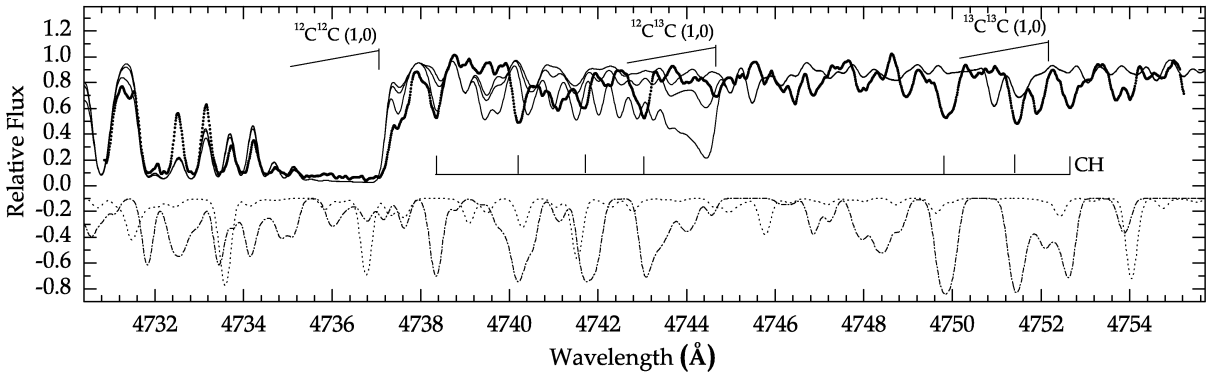

Fig. 14.— The observed spectrum of HD 112869 (solid dots), along with synthesized spectra, in the wavelength region of C_2 Swan system (1,0) bandheads. Synthesized C_2 spectra (solid lines) are shown for the final carbon abundance and three isotopic ratios, $^{12}C/^{13}C$= 90, 500, 1500. Synthesized CH (dotted-dashed line) and atomic (dotted line) spectra are presented at the bottom. CH lines identified in the observed spectrum are marked by vertical ticks.

region less blended by molecular lines and with a certain continuum definition. Mg I lines at 5167.322, 5172.685, and 5183.604 Å are synthesized to estimate the magnesium abundance. The line at 5167 Å is a significant blend, while the rest two lines are almost clean. Spectral synthesis yields the abundance $log\,\epsilon(Mg) \simeq 4.6$, with a reasonable fit for the line at 5172 Å with an equivalent width of about 360 mÅ and the line at 5183 Å with an equivalent width of about 395 mÅ (see Figure 16). Note, that the list of lines adopted for spectral synthesis contains only Mg lines, and the weak blends inside the profiles for lines at 5171 & 5183 Å were not taken into account. Thus, the magnesium abundance seems to be lower in the atmosphere of HD 112869 in comparison with the average value found for CEMP stars. A moderate magnesium overabundance, [Mg/Fe] $\simeq$ + 0.4 dex, and the absence of a significant trend of $[\alpha/Fe]$ vs. [Fe/H] were found for a large sample of CEMP stars (Allen et al. 2012 and references therein). The calculated NLTE corrections for Mg I lines (including Mg I b triplet) should not exceed +0.2 dex for the atmospheric parameters similar to those of HD 112869 (Merle et al. 2011; Mashonkina 2013). The abundance of another α-element, titanium, was found to be moderately enhanced relative to iron, [Ti/Fe] = +0.4 dex, with a tendency to provide a lower abundance from neutral lines.

Possible sources of uncertainties involved in abundance analysis are analyzed to clarify the reason of low Mg abundance found for HD 112869. The lines of Mg triplet are moderately strong and the calculated abundance can be affected by the error due to uncertainty in the adopted microturbulent velocity. The profiles of Mg triplet were synthesized for reduced microturbulence, $\xi_t = 3.0$ km s^{-1}. In this case, the Mg abundance is higher only by about 0.1 dex. The error in the abundance, produced by the uncertainty in the adopted temperature, is ±0.16 dex. The wavelength region redward of the C_2 (0,0) bandhead is free from strong molecular lines and the accuracy of continuum localization was estimated to be better than 2%. We concluded during subsequent iterations that, the local continuum should be by about 10% higher than the adopted one in order to have the magnesium abundance (log $\epsilon(Mg)$ = 5.7) observed for typical CEMP stars, [Mg/Fe] = +0.4 dex. In that case, however, the continuum should be scaled up for all lines in the wavelength region near Mg I triplet (e.g. Figures 8 and 9), what is unlikely. To characterize a total error of the calculated magnesium abundance, ±0.4 dex, the RSS uncertainty was estimated taking into account the contribution from both the random and systematic errors. Weak Mg lines should be employed to confirm our result.

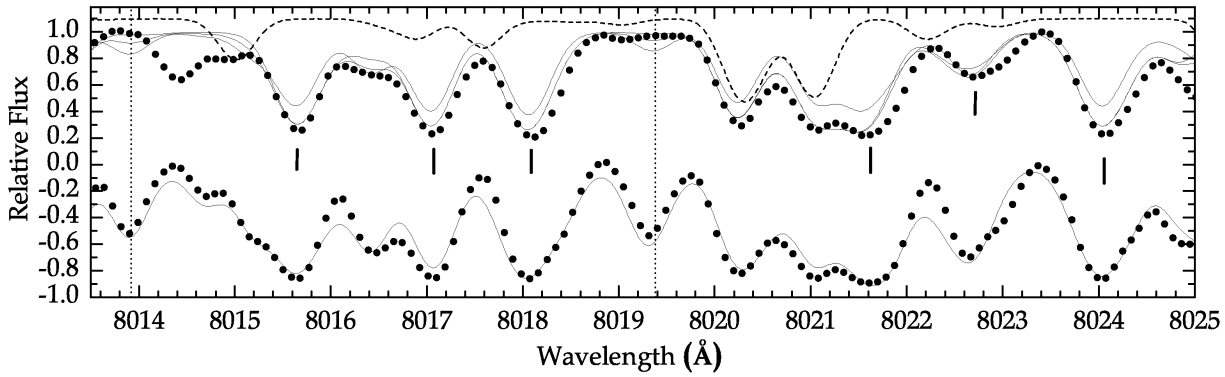

Fig. 15.— The observed spectrum of HD 112869 (filled circles on the top), along with synthesized spectra, in the wavelength region dominated by CN Red system lines. Three synthesized CN (solid line) and one C_2 (dashed line) spectra are shown for the final nitrogen and carbon abundances and the isotopic ratios $^{12}C/^{13}C$= 5, 90, 500. The positions of ^{12}CN and ^{13}CN lines are indicated by vertical ticks and dotted vertical lines, respectively. The observed (filled circles) and synthesized spectra for the comparison star HD 92055, calculated using the model parameters given in Table 1, are presented at the bottom for comparison purposes.

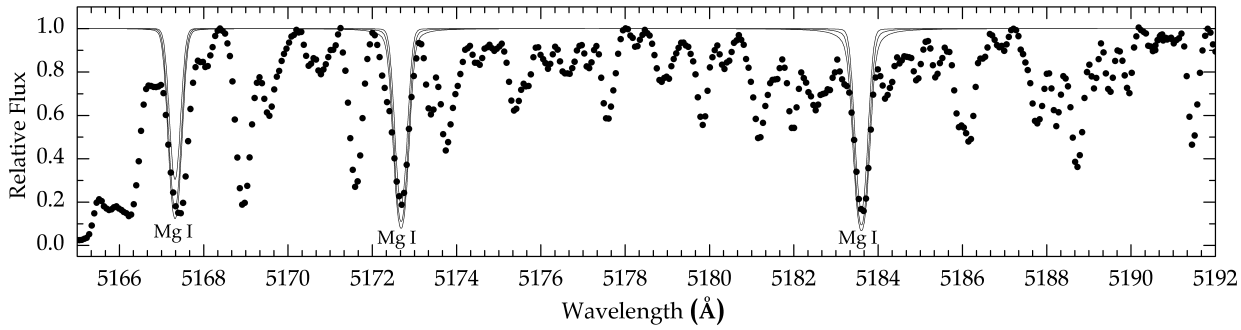

Fig. 16.— The observed spectrum of HD 112869 (filled circles), along with calculated profiles for magnesium triplet. Mg I lines are synhesized for three magnesium abundances, $log\,\epsilon(Mg)$ = 4.6, 5.3, and 5.7 dex (solid lines).

3.3.11. Neutron–capture elements

The elements formed mainly by the s-process main component can be divided into two groups: light s-process (ls) elements around the magic neutron number 50 and heavy s-process (hs) elements around the magic neutron number 82. An enhancement of the light *s*-process elements in the atmosphere of HD 112869 relative to the solar values was not confirmed. We selected two Y II lines for the abundance estimation in the wavelength region redward of the C_2 Swan system bandhead with a certain definition of the continuum level. The lines at 5200.406 and 5205.724 Å give a similar yttrium abundance within uncertainties (see Figure 17). The chromium abundance was iterated to be $log\,\epsilon(Cr) = 2.35$ using the Cr I line at 5206.023 Å which is blending with the yttrium line. The third Y II line at 4900.12 Å confirms the low yttrium abundance and an average relative abundance normalized to the iron abundance was calculated, which appears to be near zero, [Y/Fe] $\simeq 0.0$ dex. Unfortunatelly, we were not able to reproduce well C_2 and CN spectrum in the wavelength region redward of the C_2 (0,0) bandhead for the final C and N abundances because of uncertain molecular data. Therefore, the calculated atomic spectra were fitted with the observed spectrum and the iterated abundance was accepted as an upper limit of the yttrium abundance. Spectral synthesis of the strontium line at 4077.709 Å confirms the low abundance of the first s−process peak (Figure 18).

We selected a frequently employed for abundance analysis Ba II line at 6141.713 Å but, we were not able to reproduce the neighboring C_2 and CN lines using the final atmospheric model because of the uncertain molecular data (Figure 19). Again, the calculated atomic spectra were fitted with the observed spectrum and the iterated abundance was accepted as an upper limit of barium abundance, [Ba/Fe] $\lesssim -0.7$ dex. NLTE corrections for the strontium and barium lines should be lower than 0.14 dex (Short & Hauschildt 2006). The Ba II line at 4934.076 Å confirms the absence of barium overabundance, [Ba/Fe] $\simeq -0.1$ dex. Thus, two synthesized barium lines confirm a mild depletion of the heavy s−process element barium, [Ba/Fe] < -0.3 dex, on average. Spectral synthesis of two neodymium lines in the wavelength region redward of the C_2(0,0) bandhead shows the Nd enhancement (see Figure 20). Synthesis of the La II line at 4086.709 and Sm II line at 4220.660 Å confirms a similar overabundance. Thus, at least some of the elements of the second s−peak appear to be enhanced in the atmosphere of HD 112868. However, because of possibly weak unknown molecular blends we decided to be conservative and provide the upper abundance limits for the calculated neutron capture elements (Table 6). A spectrum of very high resolution is needed to update the calculated abundances and to examine the third s−process peak which should be most enhanced according the theory of nucleosynthesis of metal-poor stars (Bisterzo et al. 2010).

Our efforts to calculate the abundance of the r−process element europium was plagued by strong molecular blends and uncertain molecular data around the selected lines. The Eu II line at 6645.127 Å was selected to be the best candidate for abundance analysis. However, we concluded during our calculations that the feature identified to be the europium line is blueshifted by about 6 km s^{-1} relative to its rest wavelength. The main contributor to the feature at 6645.0 Å, measured in the spectrum of HD 112869, was identified to be the CN line at 6644.961 Å, and the Eu II line seems to be only a weak blend on the red wing of the CN line. Only a crude estimation of an upper limit of the europium abundance was possible because of uncertain oscillator strengths for the CN line at 6644.961 Å and for the neighboring C_2 lines at 6645.509 and 6645.611 Å. We modified the oscillator strengths of these three molecular lines to fit the observed profiles and then estimated the contribution of europium. A strong enhancement of r−process was denied for the atmosphere of HD 112869, [Eu/Fe] $\lesssim$ 0.8 dex (see Figure 21).

3.3.12. Comparison with the published abundances

A comprehensive calculation of the atmospheric abundance for HD 112869 from a high-resolution photographic spectrum was provided by Kipper (1992), which resulted in the abundances for 26 elements. Unfortunatelly, his results are illustrated only in two narrow wavelength ranges around C_2 bandheads and the list of employed atomic lines is absent. The iron abundance calculated by Kipper (1992) is lower that found in this paper and a difference of ∼0.6 dex seems to be mainly because of NLTE effects. Kipper (1992) calculated the iron abundance using neutral lines which are supposedly suffered from NLTE effects. Aoki & Tsuji (1997) studied the effects of metallicity for HD 112869 using SED and the best fit with the observed spectral energy distribution for this star was achieved using the model with [Fe/H] ≈ -2.0 (see Fig. 4 in Aoki & Tsuji (1997).

The carbon to oxygen ratio calculated by Kipper (1992) is typical of N-type carbon stars, C/O = 1.07, however, the adopted oxygen abundance is extremely high, $\log \epsilon$ (O) = 8.8 (see, also, comment in Aoki & Tsuji (1997)). Aoki & Tsuji (1997) obtained the C/O ratio in the range from 3.4 to 20 for six different atmospheric models with the calculated C/O value of 6.3 for the model with similar atmospheric parameters (see Table 1) and a the more reliable oxygen abundance, [O/Fe] = +0.5 dex. Thus, the C/O ratio calculated by us is in line with that calculated by Aoki & Tsuji (1997). The spectroscopic estimates of oxygen abundance for HD 112869 are still absent. Large discrepancy between the calculated nitrogen abundance (∼2.3 dex) and those by Kipper (1992) follows partly from the difference in the adopted carbon abundance. Nobody has detected molecular isotopic lines in the spectrum

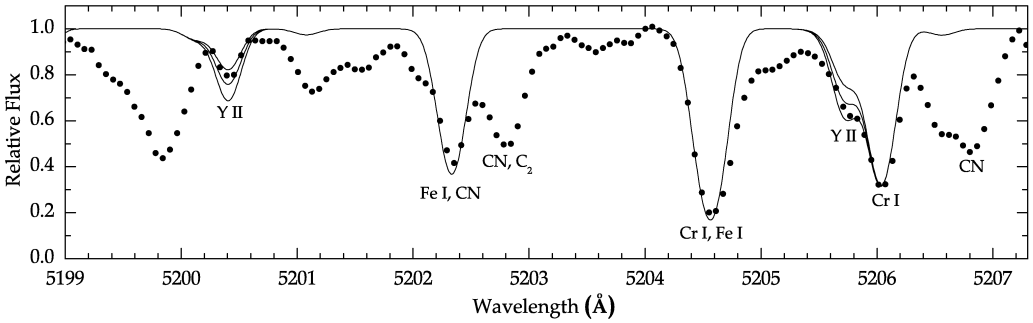

Fig. 17.— The spectrum of HD 112869 (filled circles), along with synthesized atomic spectra around Y II lines at 5200.406 and 5205.724 Å. The synthesized spectra are shown for three yttrium abundances, $log\,\epsilon(Y)$ = -0.1 ± 0.2 dex.

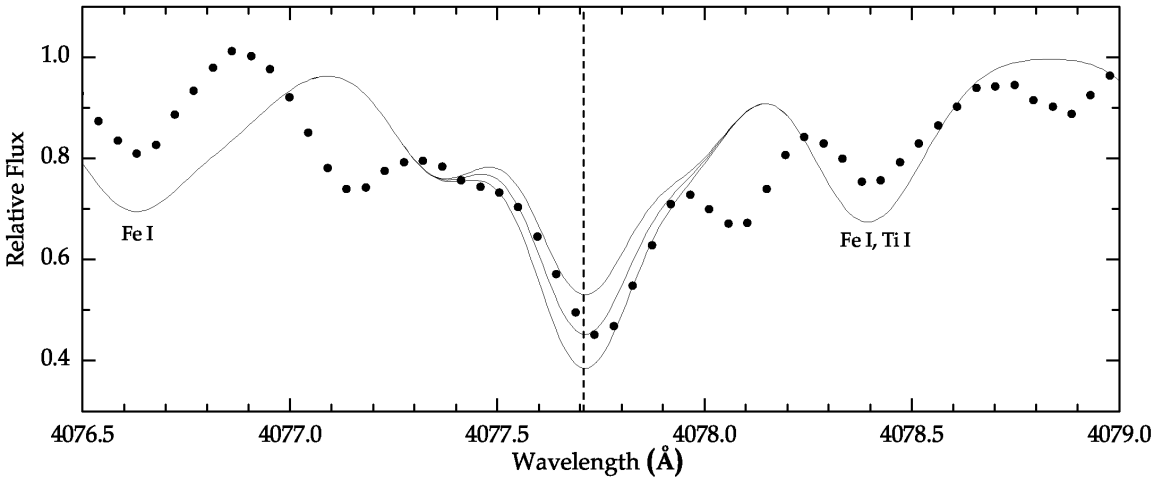

Fig. 18.— The spectrum of HD 112869 (filled circles), along with synthesized atomic spectra around Sr II line at 4077.709 Å. The synthesized spectra are shown for three strontium abundances, $log\,\epsilon(Sr)$ = -1.1 ± 0.3 dex.

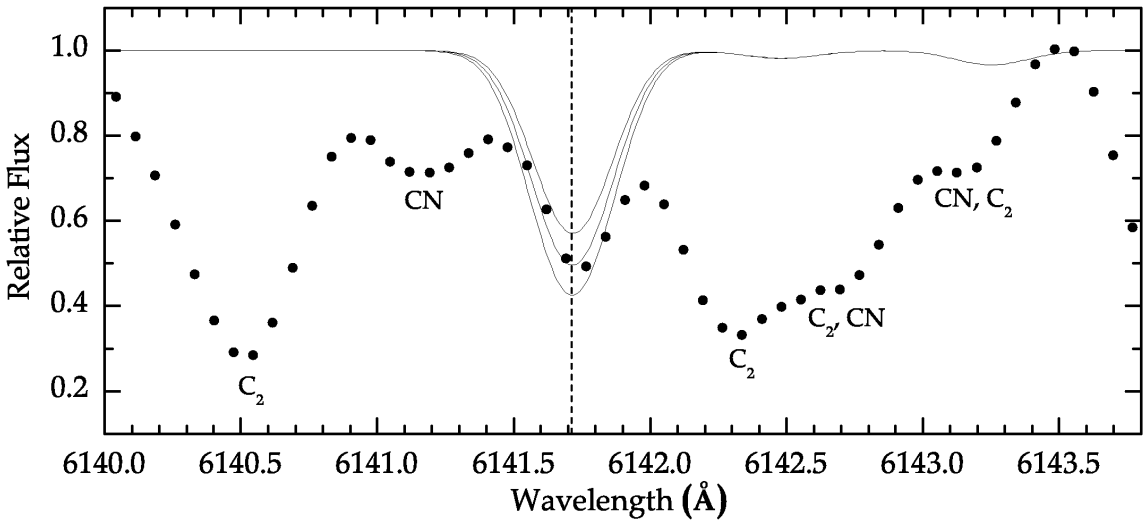

Fig. 19.— The spectrum of HD 112869 (filled circles), along with synthesized atomic spectra around Ba II lines at 6141.713 Å. The synthesized spectra are shown for three barium abundances, $log\,\epsilon(Ba)$ = -0.7 ± 0.3 dex.

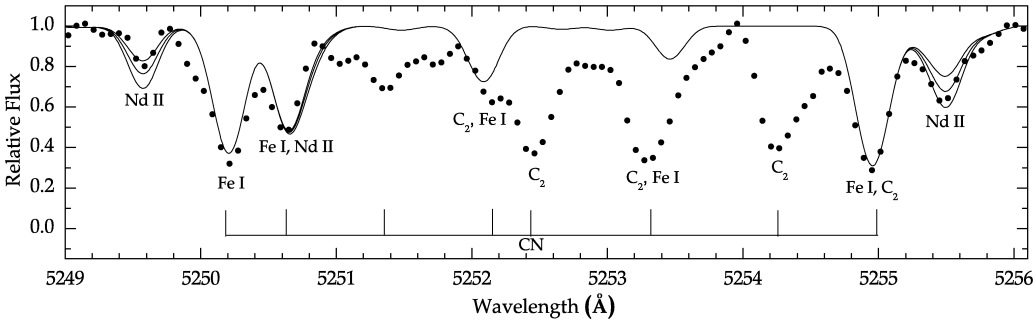

Fig. 20.— The spectrum of HD 112869 (filled circles), along with synthesized atomic spectra around Nd II lines at 5249.576 and 5255.502 Å. The synthesized spectra are shown for three neodium abundances, $log\,\epsilon(Nd)$ = -0.2 ± 0.2 dex.

of HD 112869. Spectral synthesis of the selected wavelength regions near the position of isotopic C_2 and CN lines provides a high lower limit for the carbon isotopic ratio of $^{12}C/^{13}C$ – from 50 (Kipper 1992) to 5000 (Tsuji et al. 1991; Aoki & Tsuji 1997) for six different models. Thus, our calculations are in line with the high $^{12}C/^{13}C$ ratio calculated by Aoki & Tsuji (1997).

Kipper (1992) found a large enhancement of neutron capture elements relative to the extremely low iron abundance ([Fe/H] = –2.9) in the atmosphere of HD 112869, [n/Fe] $\simeq$ +2.5 dex, on average, for 13 elements, which is in conflict with the present results. The reason of large discrepancy is not clear, however, Kipper (1992) has noted that because of heavy blending of lines the calculated abundances could be only the upper limits. Thus, the large overabundance of neutron-capture elements estimated by Kipper (1992) seems to be related to neglected molecular blending. Notice that we identified only a few relatively unblended lines of neutron capture elements in the wavelength regions where molecular contamination is lower. Notice, too, that an overestimation of s−process abundances calculated by Kipper et al. (1996) was detected for the comparison star HD 25408 (see Table 1).

4. Discussion and conclusions

The radial-velocity monitoring of HD 212869 shows variations with a peak to peak amplitude of about 10 km s^{-1} and a dominating period of about 114.9 days. The variations are semiregular, with some changes from cycle to cycle and a significant scatter of velocities near the velocity extremums, which exceeds the standard error of measurements. Similar velocity variations and scatter are observed for two protoplanetary-nebulae – HD 235858 and BD+42° 4388 (Hrivnak et al. 2013). The velocity variations of HD 112869 are accompanied by light and color variations. However, the light and color curves are shifted in phase relative to the velocity curve. The reason for the velocity, light, and color variations is obviously the pulsations in the atmosphere of HD 112869. The character of pulsations is similar to that observed for evolved stars. The dominating period agrees well with the fundamental mode calculated for luminous ($\log L/L_\odot \simeq 3.2$) and low mass (M = $0.8M_\odot$) stars in the Large Magellanic Cloud (see Figure 25 in Marigo & Girardi (2007)).

The metallicity calculated for HD 212869 is higher than that estimated prior to using high-resolution spectra. The iron abundance is found to be [Fe/H] = -2.3 ± 0.2 dex on the basis of ionised lines which are almost free from NLTE effects. The carbon abundance was found to be high in the atmosphere of HD 112869, $log\,\epsilon(C) = 8.3 \pm 0.1$ dex. The nitrogen abundance is $log\,\epsilon(N) = 6.55 \pm 0.2$ dex. With the obtained abundances [C/Fe] = +2.2 dex and [C/N] = +1.15, HD 112869 occupies the region of CEMP-s stars on the plots [C/Fe] vs.

[Fe/H] and [C/N] vs. [Fe/H] (see Figures 5 and 6 in Campbell & Lattanzio (2008). However, the s–process elements Sr, Y, and Ba are not enhanced significantly, thus confirming by definition (Beers & Christlieb 2005) the CEMP-no status of HD 112869. However, the Nd abundance seems to be enhanced relative to iron and a similar overabundance was recognized for lanthanum and samarium. From inspection of the Eu II line at 6645.127 Å, the upper limit was set for the r−process element europium, [Eu/Fe] $\lesssim +0.8$ dex. According to calculations carried out by Bisterzo et al. (2011), the abundances of three s-peaks are strongly dependent on the choice of the ^{13}C-pocket as well as on the initial mass and the metallicity. [ls/Fe], [hs/Fe] and [Pb/Fe] do not follow a linear behavior with decreasing metallicity and can cover a large range of values. For the low mass models the enhancement of the first s-process peak is low or absent. A spectrum of very high-resolution is needed to estimate the abundances for large number of the second s−process peaks and to recognize an overabundance of the third s−process peak. With the adopted oxgen abundance, [O/Fe] = +0.8 dex, the carbon to oxygen ratio was found to be very high for HD 112869, C/O $\simeq$ 12.6. The isotopic lines of C_2 and CN are too week to be detected in the crowded spectrum and the lower limit of isotopic ratio was found to be extremely high, $^{12}C/^{13}C > 1500$. A large isotopic ratio is not typical of CEMP stars. However, for low-mass AGB stars the CN processing is not expected after the second dredge-up and a total amount of ^{12}C dredged-up during the AGB phase leads to a high [C/N] ratio and a high $^{12}C/^{13}C$ ratio observed for HD 112869. On the contrary, intermediate-mass AGB stars with a hot bottom burning (HBB) should have low both [C/N] and $^{12}C/^{13}C$ ratios.

Mass transfer in a binary system or evolution of a single star on the AGB have been proposed to explain the abundance peculiarities observed for HD 112869 (Tsuji et al. 1991; Kipper 1992; Aoki & Tsuji 1997). The semiregular character of radial velocity variations accompanied by color variations rejects the binary status of HD 112869. Tsuji et al. (1991) discussed the final stages of evolution on the AGB with a small envelope mass to interpret the high C/O and $^{12}C/^{13}C$ ratios observed for HD 112869. A carbon to oxygen ratio above 1, a high luminosity and a pulsational unstability are typical features of cool evolved AGB and post-AGB stars. HD 112869, with the luminosity of $\log(L/L_{\odot}) \simeq 3.2$ and the effective temperature of $\log(T_{eff}) \simeq 3.6$, lies on the AGB of metal-poor (Z = 0.0001) low mass stars according the evolutionary tracks calculated by Bertelli et al. (2008). During thermal pulses the photospheric C/O ratio can exceed 10. The polarization observed in the visual band confirms the presence of circumstellar matter around HD 112869 (Goswami & Korinkuzhi 2013). Thus, according to the current data, HD 112869 seems to be a single metal-poor low mass TP-AGB star.

We acknowledge support from the Research Council of Lithuania under the grant No.

MIP-85/2012. The European Union FP7-PEOPLE-2010-IRSES program is acknowledged for funding exchange visits in the framework of the project POSTAGBinGALAXIES (grant agreement No. 269193). LZ thanks Drs. T.Kipper, M.R.Schmidt, U.G.Jørgensen, and A.Barzdis for assistance during the first iterations of abundance analysis and valuable discussions. This research has made use of the Simbad database operated at CDS (Strasbourg, France) and the VALD database operated at Uppsala University, the Institute of Astronomy RAS in Moscow, and the University of Vienna.

REFERENCES

Abia, C., Dominguez, I., Gallino, R., et al. 2002, ApJ, 579, 817

Abia, C., & Isern, J. 2000, ApJ, 536, 438

Allen, D.M., Ryan, S.G., Rossi, S., Beers, T.C., Tsangarides, S.A. 2012, A&A, 548, A34

Aoki, W., Beers, T.C., Christlieb, N., et al. 2007, ApJ, 655, 492

Aoki, W., Frebel, A., Christlieb, N., et al. 2006, ApJ, 639, 897

Aoki, W., Norris, J.E., & Ando, H. 2002, PASJ, 54, 933

Aoki, W., Norris, J.E., & Ryan, S.G. 2004, ApJ, 608, 971

Aoki, W., & Tsuji, T. 1997, A&A, 317, 845

Asplund, M. 2005, ARA&A, 43, 481

Asplund, M., Grevesse, N., Sauval, A.J., & Scott, P. 2009, ARA&A, 47, 481

Beers, T.C., & Christlieb, N. 2005, ARA&A, 43, 531

Beers, T.C., Preston, G.W., & Shectman, S.A. 1992, AJ, 103, 1987

Beers, T.C., Sivarani, T., Marsteller, B., et al. 2007, AJ, 133, 1193

Bergeat, J., Knapik, A., & Rutily, B. 2001, A&A, 369, 178

Bergeat, J., Knapik, A., & Rutily, B. 2002, A&A, 390, 967

Bertelli, G., Girardi, L., Marigo, P., & Nasi, E. 2008, A&A, 484, 815

Bisterzo, S., Gallino, R., Straniero, O., Cristallo, S., & Käppeler, F. 2010, MNRAS, 404, 1529

Bisterzo, S., Gallino, R., Straniero, O., Cristallo, S., & Käppeler, F. 2011, MNRAS, 418, 284

Borysow, U.G., Jørgensen, U.G., & Zheng, C.1997, A&A, 324, 185

Campbell, S.W., & Lattanzio, J.C. 2008, A&A, 490, 769

Christlieb, N., Green, P.J., Wisotzki, L., & Reimers, D. 2001. A&A, 375, 366

Depagne, F., Hill, V., Spite, M., et al. 2002. A&A, 390, 187

Eggen, O. 1972, ApJ, 174, 45

Goswami, A., & Korinkuzhi, D. 2013, A&A, 549, A68

Griffin, R. 1967, ApJ, 148, 465

Harris, G.J., Pavlenko, Y.V., Jones, H.R.A., & Tennyson, J. 2003, MNRAS, 344, 1107

Harris, G.J., Tennyson, J., & Kaminsky, B.M. 2006, MNRAS, 367, 400

Hirschi, R. 2007, A&A, 461, 571

Hrivnak, B.J., Lu, W., Sperauskas, J., et al. 2013, ApJ, 766, 116

Jørgensen, U.G., & Larsson, M. 1990, A&A, 371, 222

Keenan, P.C., & Morgan, W.W. 1941, ApJ, 94, 501

Kennedy, C.R., Thirupathi, S., Beers, T.C., et al. 2011, AJ, 141, 102

Kipper, T. 1992, BaltA, 1, 181

Kipper, T., Jørgensen, U.G., Klochkova, V.G., & Panchuk, V.E. 1996, A&A, 306, 489

Kipper, T., & Kipper, M.A. 1990, SvAL, 16, 478

Kornilov, V. G., Volkov, I. M., Zakharov, A. I., et al. 1991, Catalogue of WBVR magnitudes of bright stars of the northern sky, ed. V. G. Kornilov, Tr. Gos. Astron. Inst. im. Sternberga, 63, 400 p.

Kupka, F., Piskunov, N., Ryabchikova, T.A., Stempels, H. C.; & Weiss, W. W. 1999, A&AS, 138, 119

Kurucz, R.L., 1993, CD-ROM 1–22, Smithsonian Astrophysical Observatory

Kurucz, R.L. 2005, Mem. S.A.It. Suppl., 8, 14

Landolt, A. U. 1992, AJ, 104, 340

Lucatello, S., Beers, T.C., & Christlieb, N. 2006, ApJ, 652, L37

Lucatello, S., Gratton, R.G., Beers, T.C., & Caretto, E. 2005, ApJ, 625, 833

Marcy, G.W., & Benitz, K.L. 1989. ApJ, 344, 441

Marigo, P., & Girardi, L. 2007, A&A, 469, 239

Mashonkina, L. 2013, A&A, 550, A28

Masseron, T., Johnson, J.A., Plez, B., et al. 2010, A&A, 509, A93

Merle, T., Thévenin, F., Pichon, B., & Bigot, L. 2011, MNRAS, 418, 863

Meynet, G., Ekstrom, S., & Maeder, A. 2006, A&A, 447, 623

Nidever, D.L., Marcy, G.W., Butler, R.P., Fische, D.A., & Vogt, S.S. 2002, ApJS, 141, 503

Norris, J.E., Ryan, S.G., & Beers, T. 2001, ApJ, 561, 1034

Pavlenko, Y.V. 1997, Ap&SS, 253, 43

Pavlenko, Y.V. 2003, Astron. Zh., 80, 67

Pavlenko, Y.V., & Zhukovskaya, S.V. 2003, Kinem. Fiz. Neb. Tel, 19, 28

Piskunov, N. E., Kupka, F., Ryabchikova, T. A., Weiss, W. W., & Jeffery, C. S. 1995, A&AS, 112, 525

Samus, N.N., Durlevich, O.V., & Kazarovets, E.V. 2009, General Catalogue of variable Stars, Vizier On-Line Data Catalog

Shchukina, N.G., Bueno, J.T., & Asplund, M. 2005, ApJ, 618, 939

Short, C.I., & Hauschildt, P.H. 2006, ApJ, 641, 494

Sivarani, T., Beers, T.C., Bonifacio, P., et al. 2006, A&A, 459, 125

Sneen, C., Johnson, H.R., & Krupp, B.M. 1976, ApJ, 204, 281

Tanaka, M., Letip, A., Nishimaki, Y., et al. 2007, PASJ, 59, 939

Tsuji, T., Iye, M., Tomioka, K., Okada, T., & Sato, H. 1991, A&A, 252, L1

Udry, S., Mayor, M., Maurice, E., et al. 1999, in Precise Stellar Radial Velocities, eds. J.B. Hearnshaw & C.D. Scarfe, APS Conf., 185, 383.

Umeda, H., & Nomoto, K. 2005, ApJ, 619, 427

Upgren, A., Sperauskas, J., & Boyle, R. P. 2002, BaltA, 11, 91

van Leeuwen, F. 2007, A&A, 474, 653

Yoss, K.M., & Griffin, R.F. 1997, JApA, 18, 161

Zamora, O., Abia, C., Plez, B., Dominguez, I., & Cristallo, S. 2009, A&A, 508, 909

This preprint was prepared with the AAS LaTeX macros v5.2.

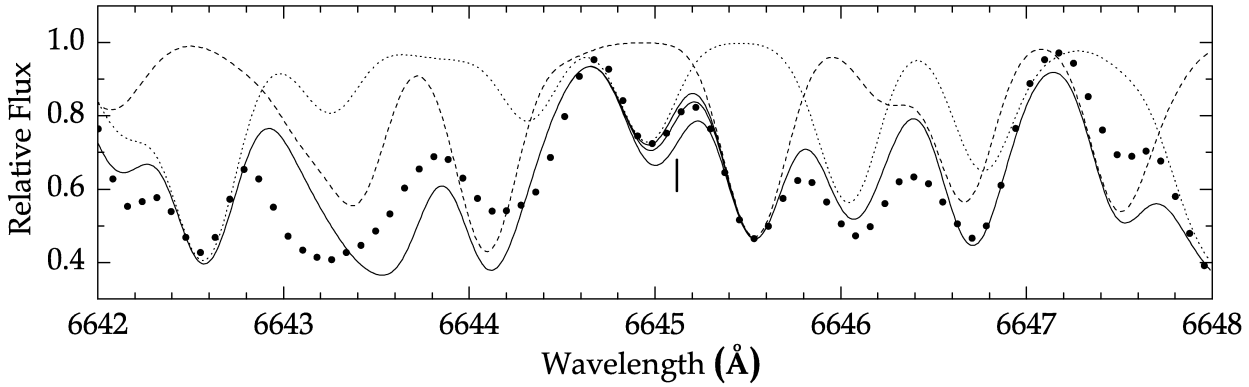

Fig. 21.— The spectrum of HD 112869 (filled circles), along with synthesized spectra around the position of Eu II line at 6645.127 Å marked by vertical tick. The latter are calculated for three europium abundances, $log\,\epsilon(Eu) = -0.5$, -1.0, and -1.5 dex (solid lines). The synthesized C_2 (dashed line) and CN (dotted line) spectra are given to illustrate the iterated molecular contribution.